PERGAMON

Journal of Structural Geology 22 (2000) 603–625

JOURNAL OF STRUCTURAL GEOLOGY

www.elsevier.nl/locate/jstrugeo

Northeastward extrusion and extensional exhumation of crystalline rocks of the Monashee complex, southeastern Canadian Cordillera

Dennis H. Johnston[a,*], Paul F. Williams[b], Richard L. Brown[c], James L. Crowley[d], Sharon D. Carr[c]

[a]*Petro-Canada Oil and Gas, P.O. Box 2844, Calgary, Alberta, Canada, T2P 3E3*
[b]*Department of Geology, University of New Brunswick, Fredericton, New Brunswick, Canada E3B 5A3*
[c]*Department of Earth Sciences, Carleton University and Ottawa-Carleton Geoscience Centre, Ottawa, Ontario, Canada K1S 5B6*
[d]*Department of Earth Sciences, Memorial University of Newfoundland, St. John's, Newfoundland, Canada A1B 3X5*

Received 19 June 1998; accepted 26 October 1999

Abstract

North American basement and cover rocks of the Monashee complex (MC) are exposed through a tectonic window within the hinterland of the southeastern Canadian Cordillera. The complex records a history of Late Cretaceous to early Tertiary crustal thickening (F_1/F_2) related to emplacement of the Selkirk allochthon (SA). Part of the MC and overlying SA then formed a mid-crustal wedge that was extruded towards the foreland from the overthickened hinterland (F_3, F_4). Finally, the complex was exhumed by Eocene ductile and brittle extensional deformation (D_5). Rocks along the studied west flank of the MC are thoroughly transposed by F_1/F_2 (into S_2). The extent of the transposition, and a well-developed northeast-trending L_2 lineation, indicate intense strain during F_1/F_2 throughout the studied portion of the MC (4–5 km thickness exposed) and overlying SA. Ductile flow continued, resulting in northeast-verging F_3 folds in the MC, west-southwest-verging F_3 folds in the SA and broad F_4 warps in the MC and SA. A shear zone records significant reactivated slip on S_2 during D_5. Rapid exhumation of the MC is attributed to ductile flow during extrusion and extensional deformation; this ductile flow is correlated with foreland thrusting, which ended in the Early Eocene.

1. Introduction

The studied area is along the west flank of the Monashee complex (Fig. 1), a basement-cored domal culmination of high-grade metamorphic rock exposed in the crystalline massifs of the Monashee Mountains of southeastern British Columbia. The Monashee complex lies within the Shuswap complex, a large area of high-grade metamorphic rock in the hinterland of the southeastern Canadian Cordillera.

Over the past two decades, it has become generally accepted (see Parrish, 1995 and references therein) that from the late Jurassic to early Tertiary, allochthonous rocks were transported towards the foreland over the Monashee complex along a northeast-directed ductile thrust fault, the Monashee décollement (Read and Brown, 1981; Brown et al., 1992). On the basis of LITHOPROBE seismic reflection profiles and surface geology, the Monashee décollement has been correlated with the basal thrust beneath the Rocky Mountain Foreland belt, providing a link between middle crustal strain in the hinterland and upper crustal strain in the foreland (Brown et al., 1992; Cook et al., 1992). To the north of the study area, along the western flank of Frenchman Cap dome, a discrete shear zone apparently defines the décollement, but to the south in the area of this study we see evidence that foreland-directed deformation was distributed through a much

* Corresponding author.
E-mail address: dejohnst@petro-canada.ca (Dennis H. Johnston).

0191-8141/00/$ - see front matter
PII: S0191-8141(99)00185-6

larger thickness of crystalline rocks (4–5 km exposed). We believe that previous interpretations of the Monashee décollement implied a foreland style of deformation that does not adequately address the strain recorded in the exposed middle crustal rocks of this part of the hinterland. The principal objective of this paper is to provide a new tectonic model for the Monashee complex in which strain was distributed through large thicknesses of middle crustal rocks as they were deeply buried and then returned to the earth's surface. We present a detailed analysis of the deformational history and new structural–metamorphic relationships and geochronological data that provide constraints on the relative and absolute timing of deformational events. Our new model integrates this deformational history both temporally and spatially into the development of the orogen as a whole.

We present structural and metamorphic evidence that northeastward thrusting and folding of crystalline rocks of the Monashee complex was accommodated by penetrative foreland-directed ductile flow which produced the regional transposition foliation. Ductile flow continued in both the Monashee complex and in the overlying Selkirk allochthon during the subsequent extrusion of a westward-tapering crustal wedge towards the foreland; the wedge was bounded above by accreted terranes of the Intermontane belt and below by North American basement. Early northeastward thrusting and the later extrusion of crystalline rocks of the Monashee complex is correlated with northeast-directed thrusting in the foreland of the Canadian Rocky Mountains (c.f. Price and Mountjoy, 1970).

2. Geological setting

The study area lies within the southern Omineca

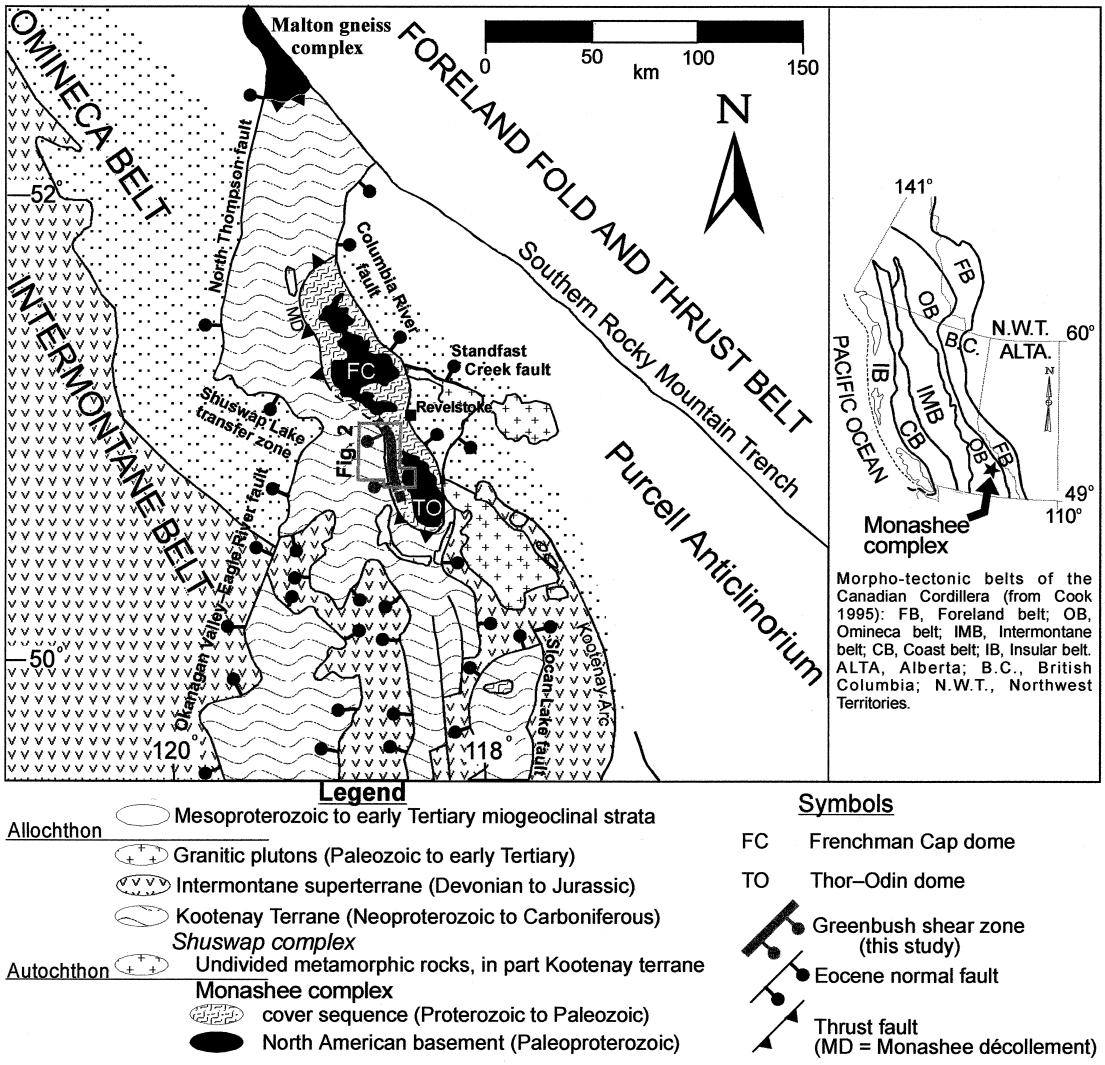

Fig. 1. Tectonic map of the southern Omineca belt (simplified from Wheeler and McFeely, 1991; Carr, 1991, 1995).

belt, the exhumed metamorphic and plutonic hinterland of the foreland fold and thrust belt of the southern Canadian Rocky Mountains (Fig. 1). The eastern Omineca belt comprises stacked and folded thrust sheets of variably metamorphosed rocks correlated with Proterozoic to Paleozoic miogeoclinal and more distal strata of ancestral North America. The western Omineca belt contains basement-cored culminations of high-grade metamorphic rocks and overlying thrust sheets and fold nappes of accreted terranes tectonically imbricated with predominately Paleozoic rocks of the pericratonic Kootenay terrane (Monger and Berg, 1984; Wheeler et al., 1991).

The Intermontane belt lies west of the Omineca belt. It consists of weakly metamorphosed Paleozoic to Lower Jurassic volcanic and sedimentary rocks of oceanic and island arc terranes accreted during northeastward obduction onto the western margin of ancestral North America in the Early and Middle Jurassic (Monger et al., 1982; Brown et al., 1986; Gabrielse and Yorath, 1991 and references therein).

The Shuswap complex and Monashee complex lie within the western Omineca belt. The Monashee complex comprises two antiformal culminations—the Frenchman Cap dome to the north of an intervening antiformal depression and the Thor–Odin dome to the south (Fig. 1). Paleoproterozoic North American basement in the cores of the culminations (Armstrong et al., 1991 and references therein; Parkinson, 1991; Crowley, 1999) is overlain by a Paleoproterozoic to Paleozoic quartzite- and marble-bearing shelf sequence (commonly referred to as the cover sequence; McMillan, 1973; Brown, 1980; Read, 1980; Scammell and Brown, 1990; see Parrish, 1995 and Crowley, 1997a for U–Pb age constraints). The Monashee complex is conspicuously devoid of Paleozoic to Tertiary granitic plutons that otherwise occur throughout the rest of the Omineca belt (Parrish et al., 1988). Proterozoic to Triassic rocks structurally overlying the Monashee complex have been assigned to the Selkirk allochthon (e.g. Read and Brown, 1981; McNicoll and Brown, 1995; Parrish, 1995; Fig. 1).

Both the Shuswap and Monashee complexes are presently bounded by major faults (Fig. 1). The Shuswap complex is bounded by Eocene normal faults, the west-dipping Okanagan Valley–Eagle River fault system (Tempelman-Kluit and Parkinson, 1986; Parrish et al., 1988; Johnson, 1994; Johnson and Brown, 1996) and the east-dipping Columbia River fault system (Read and Brown, 1981; Parrish et al., 1988; Lane et al., 1989). Rocks in the immediate hanging wall of these normal faults are generally lower-grade and were much cooler in the Eocene than their high-grade counterparts in the footwall (Parrish et al., 1988; Parrish, 1995). As pointed out above, the Monashee complex has been interpreted as being bounded above by a major northeast-directed ductile thrust fault—the Monashee décollement—which is said to separate the Monashee complex from the larger Shuswap complex. At the northwestern margin of the Monashee complex, the Monashee décollement (MD) is described as a 1–2-km-thick zone of intense ductile strain and interpreted as being part of a crustal-scale thrust duplex (Journeay and Brown, 1986; Brown et al., 1992; Cook et al., 1992). At the southwestern margin of the Monashee complex, the MD is described as an approximately 2-km-thick sheared zone that contains isoclinal folds and imbricate thrust slices (McNicoll and Brown, 1995). On the east side of the Monashee complex, Lane et al. (1989) correlated a 1-km-thick zone of annealed top-to-the-east mylonites along the Columbia River near Revelstoke with annealed top-to-the-east mylonites on the west margin of the Monashee complex (MD mylonites of Journeay and Brown, 1986). Lane et al. (1989) also concluded that post-peak-metamorphic top-to-the-east mylonites along the Columbia River could be correlated with either or both Late Cretaceous to Paleocene movement on the MD (Journeay and Brown, 1986) or with Eocene normal displacement on the Columbia River fault. Parrish et al. (1988) argued that greenschist facies top-to-the-east mylonites subjacent to the Columbia River fault are of Early Eocene age (ca. 55 Ma) and of extensional origin. We do not recognise the MD as a narrow shear zone. If it does exist, it is a cryptic pre-F_3 structure compatible with the extrusion model put forward in this paper.

3. General lithology

The eastern portion of the study area (e.g. Davis Peak, Blanket Mountain, Fig. 2) is dominated by metasedimentary rocks of the cover sequence. The cover sequence includes distinctive quartzites and marbles and thick heterogeneous paragneiss units of predominately calc-silicate gneiss and lesser proportions of pelitic schist. Basement gneiss and granitic orthogneiss units are structurally interlayered with this shelf sequence (Fig. 2).

Between Three Valley Lake and Grizzly Flats, orthogneiss units correlated with basement as well as granitic and dioritic orthogneisses occur within thick sequences of heterogeneous paragneiss (predominately psammitic–pelitic and calc-silicate gneiss); thin interlayers of quartzite and marble are rare (Fig. 2). This heterogeneous assemblage of gneisses occurs across a wide area between Victor Lake and Three Valley Lake, but narrows considerably southward towards Grizzly Flats. This narrowing may be due to steeper dips in the south rather than significant differences in thickness.

Thick units of quartzite and marble are exposed on

the east slopes of Joss Pass, at Frog Falls and in the Joss Mountain alpine area, interlayered with calc-silicate gneiss, granitic orthogneiss and rare pelitic schists (Fig. 2). Thick sheets of granitic, locally granodioritic, orthogneiss are well exposed around Joss Mountain. Interlayered psammitic–pelitic gneiss and pelitic schist occur west of Joss Mountain.

Boudins and interlayers of amphibolitic gneiss, and variably deformed boudins and interlayers of pegmatite, are very common in gneisses and schists throughout the area. Vertical to subvertical, undeformed, post-metamorphic lampropyhre, pegmatite and aplite dykes cut all rock types.

The whole sequence is thoroughly disrupted by transposition on all scales. Thus all units are lenticular. On the basis of regional correlations only, a

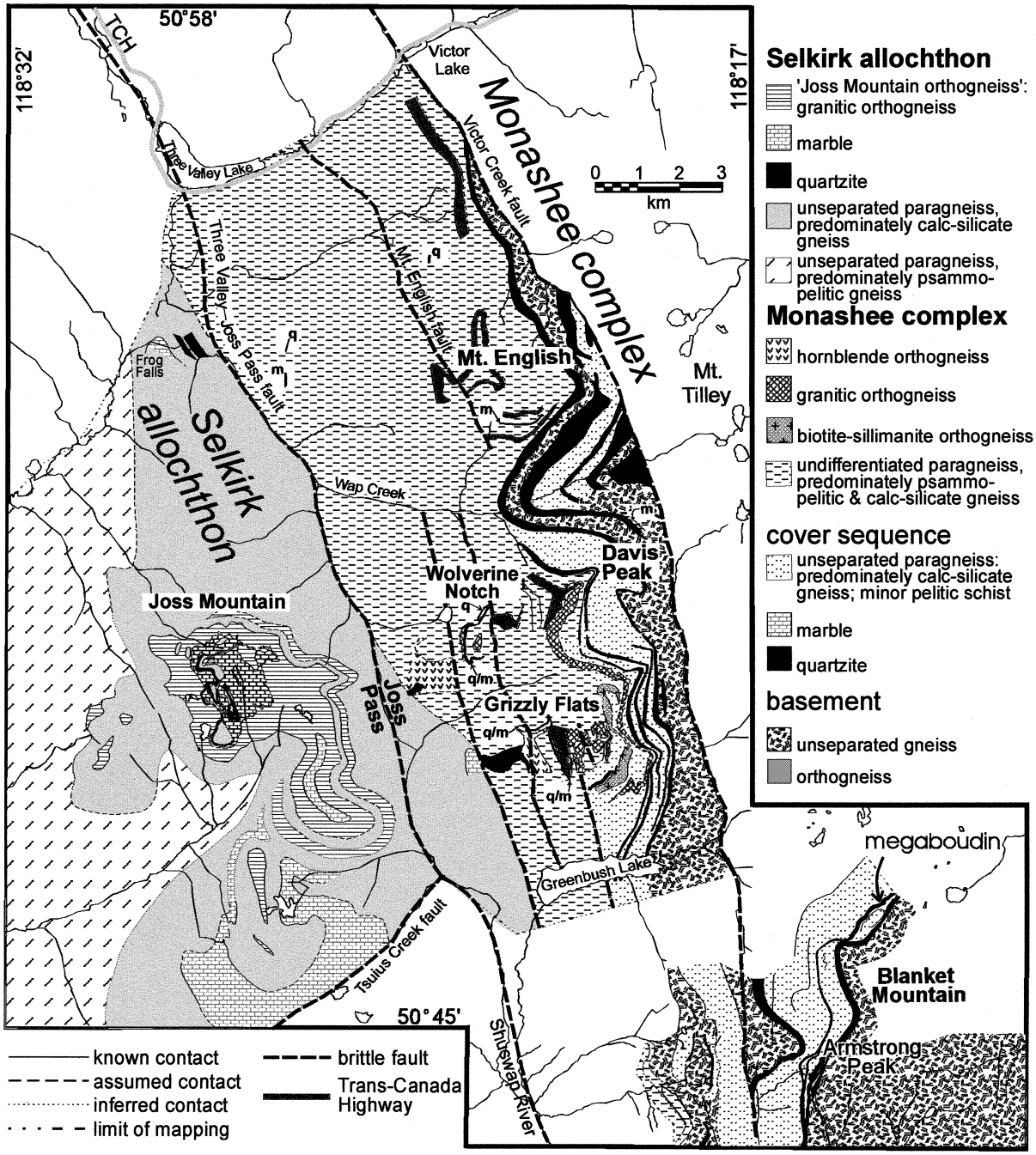

Fig. 2. Simplified geological map of the northwest portion of the Thor–Odin dome, Monashee complex. Geology of the southwest Mt. English area per Read and Klepacki (1981); geology of the Armstrong Peak area per Spark (1999). Wolverine Notch and Grizzly Flats are informal place names used in this study.

Table 1
Summary of the prominent features of the deformational history proposed for the study area

Deformation event	Structures	Fold vergence/shear sense
F_1/F_2	Tight folds intrafolial with respect to the regional transposition foliation, S_2; shears at low angles to S_2; intersection lineation, L_{2i}	Vergence: predominately NE. Shear: top-to-the-NE.
F_3	Open to tight asymmetric folds; weak L_3	Vergence: SW in Selkirk Allochthon, NE in Monashee Complex.
F_4	Upright open folds; broad warps	None
D_5—ductile	Shear bands; folds and dykes truncated by reactivated slip on S_2; L_5	Shear: top-to-the-WSW
D_5—brittle	West- and rare east-dipping normal faults; right lateral oblique-slip faults	

gradational lithostratigraphic succession is tentatively proposed for the west flank of the Thor–Odin dome: predominately basement and cover sequence units within the Monashee complex in the east pass westward to predominately Selkirk allochthon units in the west (Fig. 2). However, until more depositional and igneous ages are known, even this crude succession must be viewed with caution.

4. Deformational history

4.1. Introduction

The most prominent structural feature in the gneisses and schists in the study area is a regional foliation, which is folded to form the Thor–Odin dome. In general, two groups of folds can be distinguished: those that are intrafolial with respect to the regional foliation (F_1/F_2 folds) and those that fold the regional foliation (F_3 and F_4 folds). These F_1 to F_4 folds are overprinted by late ductile and brittle extensional deformation (D_5). F_1/F_2 to D_5 deformational events are outlined in Table 1.

4.1.1. Main foliation: F_1/F_2 and the development of S_2

The prominent foliation in gneisses and schists, defined by compositional layering (possibly bedding) and the preferred orientation of platy minerals (e.g. micas), is a typical transposition foliation (in the sense of Sander, 1911; c.f. Hobbs et al., 1976; Williams, 1983; Williams and Campagnoni, 1983). On the basis of structural overprinting, at least two generations of folds (F_1 and F_2) are intrafolial with respect to this foliation and are interpreted as having contributed to its development. Tight to isoclinal folds (F_2) that refold earlier-formed isoclinal folds of (F_1) migmatitic layering are common. Layering is typically thickened in the hinges of intrafolial folds and thinned or attenuated on the limbs (e.g. Fig. 3); pinch-and-swell structures commonly comprise attenuated limbs and thickened hinges, respectively. S_2 is commonly cut by mesoscopic shear surfaces or zones that generally make an acute angle with S_2 (*cut-offs* of Bell and Etheridge, 1973). The orientation of the truncations with respect to the main foliation consistently indicates that these structures formed as shear bands as a result of top-to-the-northeast S_2-parallel shear. Although overprinted by a later recrystallization, top-to-the-northeast shears are commonly preserved, particularly in pelitic schists. We thus label the principal foliation S_2 and correlate it with the transposition foliation recorded elsewhere in the Monashee complex (e.g. Carr, 1991; Scammell, 1993; Johnson, 1994).

The orientation of S_2 in the studied western margin of the Thor–Odin dome is shown in Fig. 4. S_2 dips consistently to the west-southwest throughout a 2.5-km-thick panel of crystalline rock that is exposed in cliffs rising from the valley floor of the Victor Creek fault lineament to summits immediately west (e.g. Davis Peak), and in the ridges which extend west-

Fig. 3. View west-southwest of F_1/F_2 isoclinal folds of a garnet-rich amphibolite layer in calc-silicate gneiss, Grizzly Flats. Note the thickened hinges and thinned and attenuated limbs of the F_1/F_2 folds and the numerous low-angle cutoffs.

southwest from these summits (Fig. 4, domains C and C′). This panel, referred to here as the Davis Peak panel, dominates the central portion of the study area.

In the central and lower levels of the Davis Peak panel, shear planes that transect S_2 at shallow angles are very common; the shear planes are overprinted by a later pervasive recrystallization. These metre-scale shears are the most conspicuous indication of top-to-the-northeast movement on S_2. In this same zone, smaller shears, commonly spaced 1 cm or less apart, are locally well developed in pelitic schists. Deflection of S_2 into these small shears produced a penetrative top-to-the-northeast 'shear band foliation' (White et al., 1980; e.g. Fig. 5). C/S fabric (Berthé et al., 1979; Lister and Snoke, 1984) occurs in pelitic schists at low structural levels (e.g. Blanket Mountain;

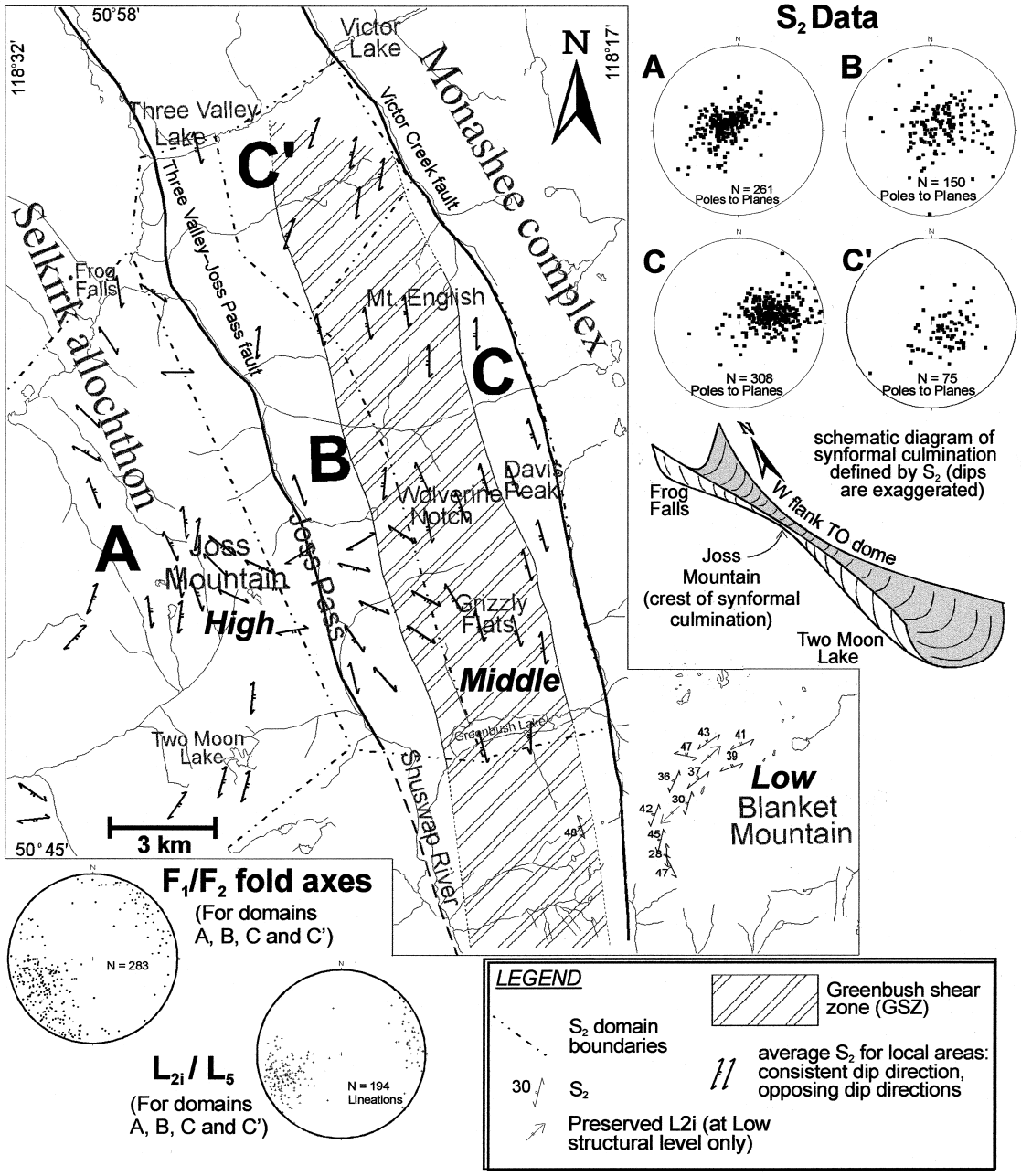

Fig. 4. Structural data for the study area. S_2 data are shown for domains A, B, C and C′; S_2 foliations are shown for the Blanket Mountain area. Average S_2 foliations for local areas are shown to outline the large-scale synformal culmination of the regional foliation that occurs along the northwest flank of the Thor–Odin dome. Poles to S_2 are shown in equal area lower hemisphere projections. Equal area lower hemisphere projections of F_1/F_2 fold axes and L_{2i}/L_5 lineations are for domains A, B, C and C′ only. Low, middle and high are structural levels defined with respect to the Davis Peak panel (domains C and C′) and the GSZ.

c.f. Spark, 1999). The widespread occurrence of top-to-the-northeast fabrics, from Joss Pass to low structural levels of the Thor–Odin dome, and the lack of any recognizable change in the pre-D_5 fabric, indicate that pre-D_5 top-to-the-northeast shear was distributed throughout the whole of this part of the Thor–Odin dome.

Because compositional layers are commonly truncated along strike, and because F_1 and F_2 folds have similar styles, intrafolial folds can only be designated F_1 or F_2 with certainty where overprinting relationships exist. For this reason, tight to isoclinal, intrafolial folds are designated F_1/F_2. These F_1/F_2 folds are typically disharmonic and commonly have varying amplitudes along their hingelines. They have an axial plane foliation defined by grain shape and mineral orientation.

Within the central and upper portions of the Davis Peak panel, there is a zone of west-southwest-dipping, top-to-the-west-southwest shear bands referred to here as the Greenbush shear zone (GSZ, described below in discussion of D_5 structures). The GSZ is introduced here because it is useful for the purposes of this study to distinguish structural levels relative to the GSZ and the Davis Peak panel (Fig. 4). The Davis Peak panel is considered a middle structural level. At 'low' structural levels, below the Davis Peak panel, both the strike and dip of S_2 vary (e.g. Blanket Mountain; Fig. 4). At 'high' structural levels, west of the Thor–Odin dome and above the GSZ, S_2 defines a large open synformal culmination which trends north-northwest (S_2 domains A and B, Fig. 4); the crest of the synformal culmination occurs in the Joss Mountain alpine area.

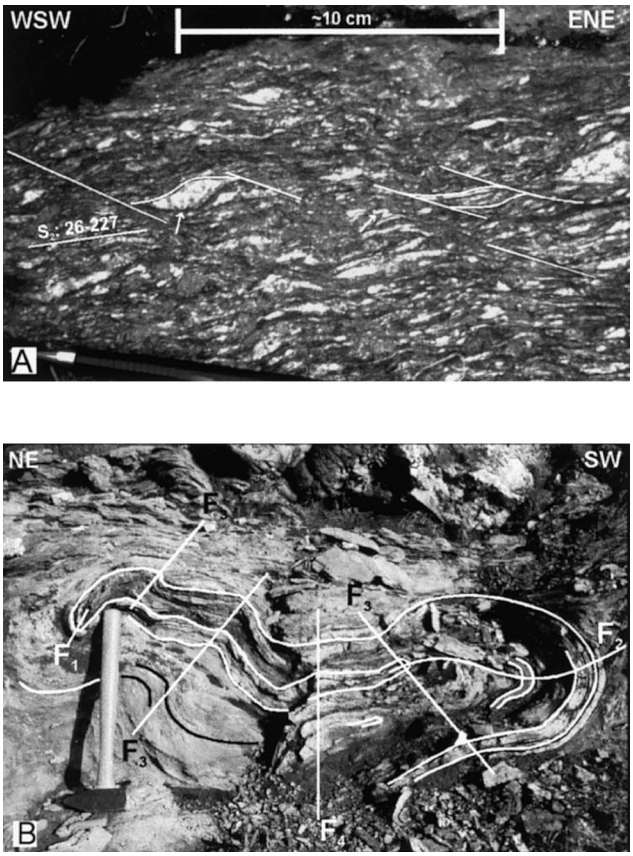

Fig. 5. (a) View towards 335° of F_1/F_2 shear bands in pelitic schist, Wolverine Notch; deflection of S_2 indicates top-to-the-northeast shear. Asymmetric microfolds and asymmetric feldspar porphyroclasts also indicate top-to-the-northeast shear (arrows). (b) View southeast of overprinting relationships between F_1, F_2, F_3 and F_4 folds, Joss Mountain (c.f. Fig. 7).

F_1/F_2 hinges (Fig. 4a) generally trend west-southwest along the west flank of the Thor–Odin dome (e.g. Grizzly Flats, Joss Mountain; Fig. 3) and northeast at lower structural levels towards the core of the culmination (e.g. Blanket Mountain) where rare northeast-trending sheath folds have been observed. Asymmetric F_1/F_2 folds are very common; most are north-verging although there are small domains where F_1/F_2 folds are south-verging (c.f. Craig, 1966; Read and Klepacki, 1981; Duncan, 1984; McNicoll and Brown, 1995).

Boudins formed during F_1/F_2 are common, and, where there is a large competency contrast (e.g. amphibolite in schist), the boudins are commonly terminated by inclined surfaces suggestive of Riedel shears. These surfaces dip north indicating top-to-the-north shear on S_2. They vary considerably in orientation as do F_1/F_2 boudin neck folds. F_1/F_2 boudins occur on all scales and include some of leviathan proportions (e.g. the km-scale boudin at Blanket Mountain, Fig. 2).

The intersection of tight to isoclinally folded layering and an S_2-parallel axial plane foliation results in a penetrative intersection lineation (L_{2i}) along the west flank of the Thor–Odin dome. L_{2i} is generally colinear with the hinges of F_1/F_2 folds. In rare cases, L_{2i} is defined by hingelines of reclined F_1/F_2 microfolds exposed on S_2. Elongate aggregates of quartz (rods) are well developed locally and are parallel to F_1/F_2 fold axes.

Northeast-trending L_{2i} is preserved at low structural levels (Blanket Mountain) where it is parallel or slightly inclined to an L shape fabric in quartz and feldspar. At higher levels farther west, L_{2i} is rotated to a west-southwest trend by D_5 (e.g. Grizzly Flats).

4.1.2. Significance of F_1/F_2 structures

In rocks below the Davis Peak panel, rare sheath folds, a shape fabric, and rodding indicate a northeast-trending stretching direction, at least during the late stages of the development of S_2. The orientation pattern of F_2 folds is consistent with this interpretation; some are at a high angle to the stretching lineation, but most approach parallelism. There is a tendency for the tighter folds to be the ones most nearly parallel to the lineation (c.f. Mawer and Williams, 1991). These

observations are consistent with the folds having developed as dragfolds with northwest trends and having rotated during continuing shear towards the northeast. Early-formed Riedel shears, associated with boudin development, have also been rotated, by variable amounts, towards the stretching direction. Late-formed shear bands mostly strike approximately perpendicular to the movement direction.

At middle structural levels, as the GSZ is approached, the F_1/F_2 structures described above are modified by D_5 deformation, and the earlier kinematic relationships preserved at low structural levels are obscured. Nevertheless, the F_1/F_2 fabric observed throughout the Davis Peak panel is similar to the fabric observed in rocks at low structural levels, indicating that the whole of the studied area along the west flank of the Thor–Odin dome underwent the same transposition. Given that the zone is at least 4 km thick, we believe that the minimum displacement of the hanging wall relative to the footwall would have to be tens of kilometres to explain the observed fabric (c.f. Williams and Zwart, 1977). The presence of Riedel shears and the ductile equivalent, shear bands, indicates that the top-to-the-northeast shear was accompanied by a component of S_2-normal shortening (c.f. Williams and Price, 1990).

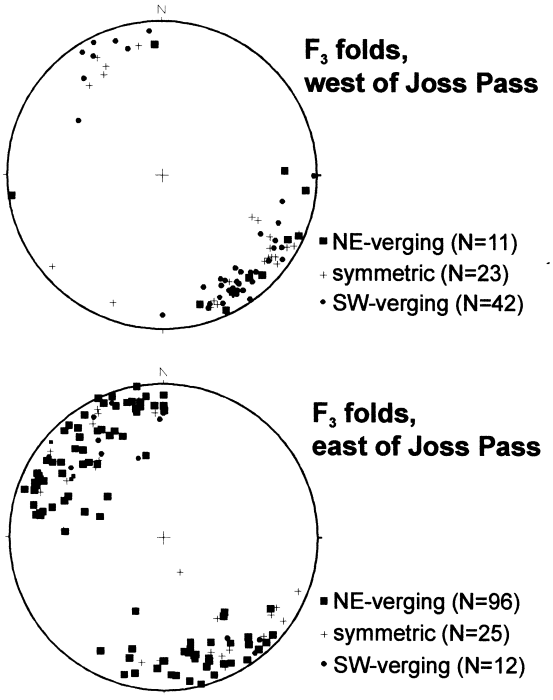

Fig. 6. Equal area lower hemisphere projections of F_3 fold axes east and west of Joss Pass. F_3 orientation data are for domains A, B, C and C′ (see Fig. 4). Note that rare asymmetric folds classified as NE-verging actually verge north or east and that rare asymmetric folds classified as SW-verging actually verge south or west.

4.2. F_3 and F_4 folds

F_3 folds are open to tight and generally lack an axial planar foliation. In most cases, coarse-grained minerals that define S_2 and are folded around F_3 hinges are recrystallized (e.g. sillimanite). Locally there are good overprinting relationships between F_1/F_2 and F_3 folds (e.g. Fig. 5b). Where overprinting does not exist, distinguishing F_1/F_2 folds from F_3 folds can be difficult, particularly where D_5 extensional deformation is intense. Statistically, there appears to be a trend from tight to isoclinal F_1 folds through closed to isoclinal F_2 folds that generally plunge northeast or southwest, to open to closed F_3 folds that plunge northwest or southeast. Locally, L_{2i} is folded by F_3. Pervasive recrystallization occurred after F_3 folds had formed. Thus F_1/F_2 folds generally cannot be distinguished from F_3 folds on the basis of their relationship to the thermal metamorphic peak assemblages.

At low structural levels (e.g. Blanket Mountain), F_3 folds are more easily distinguished from F_1/F_2 on the basis of style. They trend east–west and are north verging (c.f. Craig, 1966). At middle structural levels farther west, between the Victor Creek fault and Joss Pass, shallow doubly plunging F_3 folds are northwest-trending and predominately northeast-verging (c.f. Journeay, 1986). There is a major F_3 vergence reversal across Joss Pass (Fig. 6; c.f. Carr, 1991). West of Joss Pass, shallow doubly-plunging F_3 folds are also northwest-trending, but predominately verge to the southwest (c.f. Johnson, 1994). Kilometre-scale west-southwest-verging folds were mapped at Joss Mountain (Fig. 7).

At Blanket Mountain, kyanite overprints F_1/F_2 folds and occurs randomly on S_2 surfaces that are folded in turn by open F_3 folds. Crystals, 5–10 cm in size, of kyanite are locally bent gently around F_3 hinges but mostly the crystals are straight, indicating F_3 folded rigid kyanite crystals. The kyanite was pseudomorphously replaced by fine-grained sillimanite. Locally there is a weak lineation (L_3) parallel to the F_3 hinges defined by the subparallel alignment of the kyanite pseudomorphs.

At low structural levels of the Thor–Odin dome, upright north-trending F_4 folds are open to closed and have variable plunges. At middle and high structural levels, upright north-trending F_4 folds are gentle to open with gentle northerly plunges.

4.3. Extensional deformation (D_5)

4.3.1. Greenbush shear zone (GSZ)

There are spectacular exposures of steep west-southwest-dipping, top-to-the-west-southwest shear bands (e.g. Fig. 8) on the south-facing slopes of east–west ridges from Mount English south to the Greenbush Lake area (Fig. 3). The shear bands are concentrated in a 1.5–2-km-

thick zone within the upper portion of the Davis Peak panel. The strike of the D_5 shear bands follows that of S_2. At Mount English, the strike of S_2 and the shear bands changes from north-northwest to north-northeast into the antiformal depression linking the Thor–Odin and Frenchman Cap culminations. Back-rotation of S_2 between shear bands occurs in some exposures, resulting in local east-dipping panels of S_2 between west-dipping shear bands. Discrete late metamorphic extensional shear zones have been recognized elsewhere along the western flank of the Monashee complex (Journeay, 1986; Brown et al., 1986; Scammell, 1986), and these zones may be evidence of continuation of the GSZ to the north and south of the study area.

The shear bands commonly die out along strike, collectively forming an interleaving array. Their length

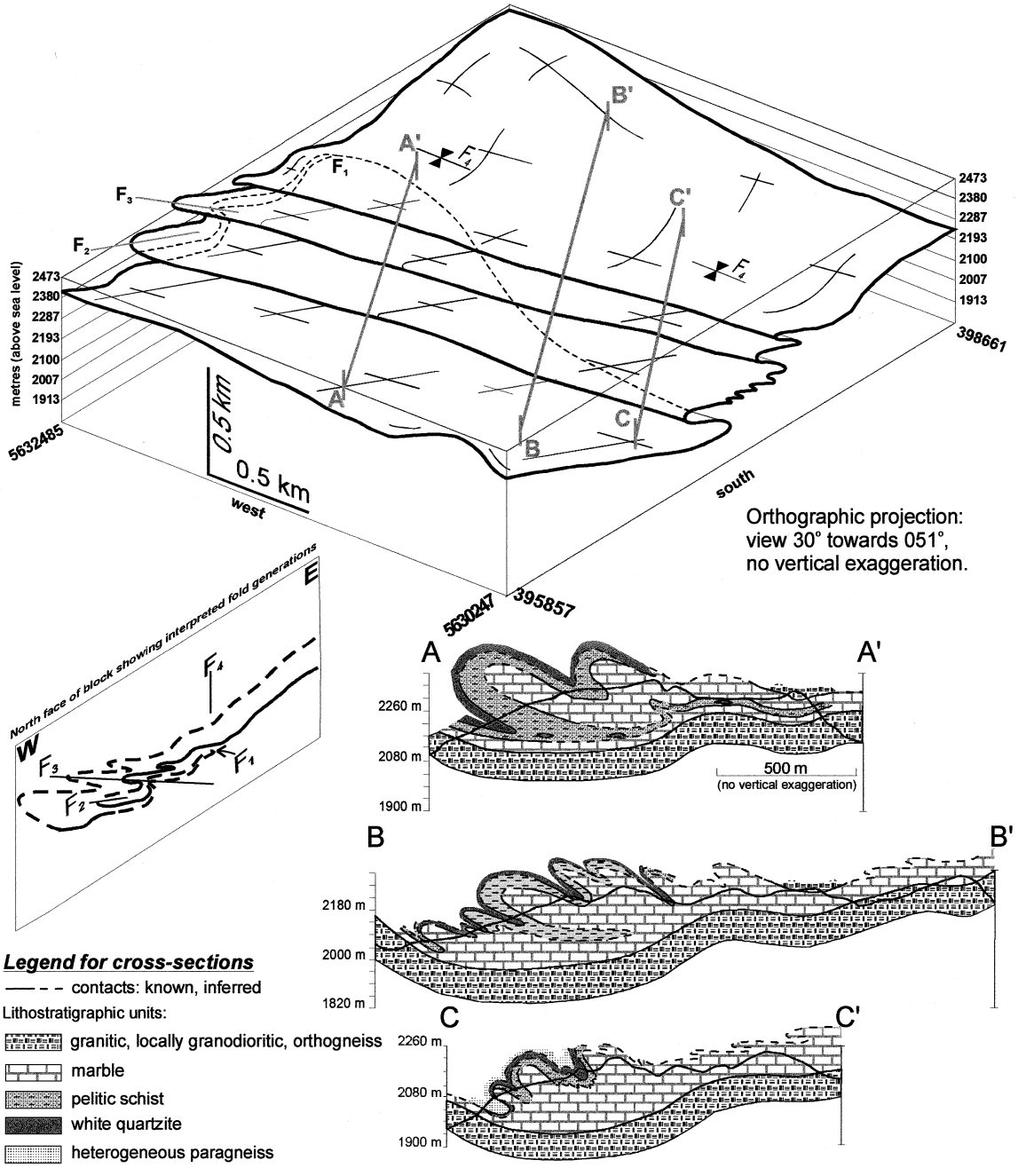

Fig. 7. Block diagram and cross-sections of the km-scale southwest-verging Joss Mountain F_3 folds. The block diagram is of the pelitic schist/marble contact surface. Locations of the three cross-sections shown were selected on the basis of where the best F_1 and F_3 infolds of quartzite and pelite into marble are exposed on the west slopes of Joss Mountain. The vertical cross-sections are approximately profiles of the F_3 folds. Compare interpreted F_1 with F_4 overprinting with Fig. 5(b).

along strike ranges from metres to hundreds of metres. They are steeply west-southwest-dipping, typically cutting down through the regional foliation from 1 to 5 m and merging top and bottom into the regional foliation (e.g. Fig. 8). Rare larger shear bands occur (e.g. > 100 m at Wolverine Notch); their maximum size is not known.

The GSZ is characterized by a strong west-southwest-trending stretching lineation (L_5) on S_2/S_5. L_5 is a composite of rotated and stretched L_{2i} and L_3, and of newly developed metamorphic minerals (most notably sillimanite, which commonly has pseudomorphously replaced kyanite). In the GSZ, there are rare occurrences of preserved north-trending L_{2i} sweeping to a westerly trend. Rotation of the north-trending lineation to a west-southwest trend as the GSZ is approached is evident at a larger scale in the lineation data of Spark (1999): from east to west across the southern slopes of Armstrong Peak, the lineation gradually changes from a north to a west-southwest trend. This rotation of the lineation is interpreted as D_5 overprinting of L_{2i} as the GSZ is approached. The strong D_5 deformation also obscures the F_3 folding of rigid kyanite crystals and the L_3 lineation recorded at low structural levels. Sillimanite grains or bundles, which commonly define L_5, are boudinaged and pull-aparts are filled in with muscovite ($\pm$biotite, $\pm$chlorite). Sillimanite defining L_5 is predominately recrystallized, indicating sillimanite-stable temperatures during much of the L_5 development history. Muscovite, biotite and chlorite infilling of L_5 pull-aparts is interpreted as having occurred during brittle–ductile D_5 deformation, contemporaneous with the final stages of shear band development.

It is commonly difficult to distinguish L_5 and L_2 along the west flank of the Thor–Odin dome. There is a slight, yet discernible difference in the trend of the two lineations: L_5 trends west with a spread to the west-southwest whereas L_2 trends southwest with a spread to the west-southwest. There are rare F_3 folds that fold L_{2i}. However, F_3 folds have never been seen to fold a mineral lineation, suggesting the ubiquitous mineral lineation formed after F_3. Whereas there is evidence at low structural levels that replacement of kyanite by sillimanite postdated F_3, at middle structural levels this relationship is obscured by D_5. Thus, relatively high temperature/low pressure metamorphic conditions prevailed after F_3 folds formed, converting kyanite to sillimanite, and persisted as L_5 developed.

The common occurrence of the shear bands within the GSZ, many of which have offset layers with dip separations of tens of metres or more, indicates significant D_5 reactivated slip on S_2 (Williams and Price, 1990; see independent evidence of D_5 slip cited below). This interpretation is supported by the presence of the strong west-southwest-trending L_5 stretching lineation in the GSZ. The preponderance of shear bands within the GSZ also indicates significant thinning occurred perpendicular to S_2 across the zone. However, only westerly dipping shear bands are well developed, rather than a conjugate set, indicating that top-to-the-west-southwest S_2-parallel shear was strong relative to S_2-normal shortening (c.f. Williams and Price, 1990).

There are rare F_3 folds truncated by the reactivated slip on S_2 surfaces. Tourmaline-bearing pegmatite dykes, contemporaneous with D_5, cut S_2 but in rare instances are sheared by reactivated slip along discrete S_2 surfaces during D_5. Boudinage occurred as a result of this reactivated slip (e.g. Fig. 8). Neck folds of D_5 boudins trend approximately north–south; boudinage of F_1/F_2 boudins has been observed in rare well-exposed, three-dimensional outcrops. The common occurrences of D_5 shear bands and boudins and the rare occurrences of truncated F_3 folds and dykes sheared along the regional foliation indicate that there was significant reactivated slip on S_2 during D_5.

Normally there is localized alteration of biotite to chlorite and sillimanite to fine-grained white mica within D_5 shear bands. Thin solution seams, rich in Fe-oxides, commonly define C' in microscopic-scale C'/S fabrics within mesoscopic shear bands. Thus, fluids probably coursed through most shear bands during or after their formation.

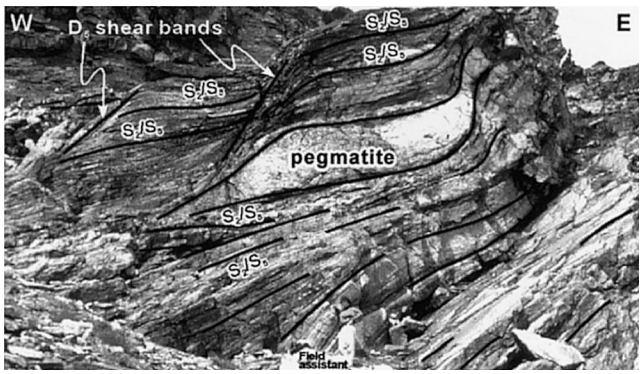

Fig. 8. View north of top-to-the-west-southwest D_5 shear bands of the Greenbush shear zone, Grizzly Flats.

4.3.2. Brittle faults

Large subvertical north-northwest-trending faults mapped along the west flank of the Thor–Odin culmination include the Three Valley normal fault (Jones, 1959; Johnson, 1994; this study) and the right-lateral oblique-slip Victor Creek fault (Read, 1980; this study; see Fig. 2). Slickenside striae and offsets indicate predominately dip-slip displacements on both east- and west-dipping normal faults. The common occurrence of brittle faults suggests that they played an important role in the extensional exhumation of the Monashee complex, possibly rivalling the role of the D_5 ductile extension.

5. Metamorphism

5.1. General comments

Rocks throughout most of the study area were at upper-amphibolite facies, indicated by a metamorphic assemblage of K-feldspar, sillimanite and melt in migmatitic pelitic schists and psammo-pelitic gneisses. Lower to middle amphibolite facies peak-metamorphic conditions prevailed at high structural levels (Joss Mountain; Fig. 7), below the muscovite-breakdown

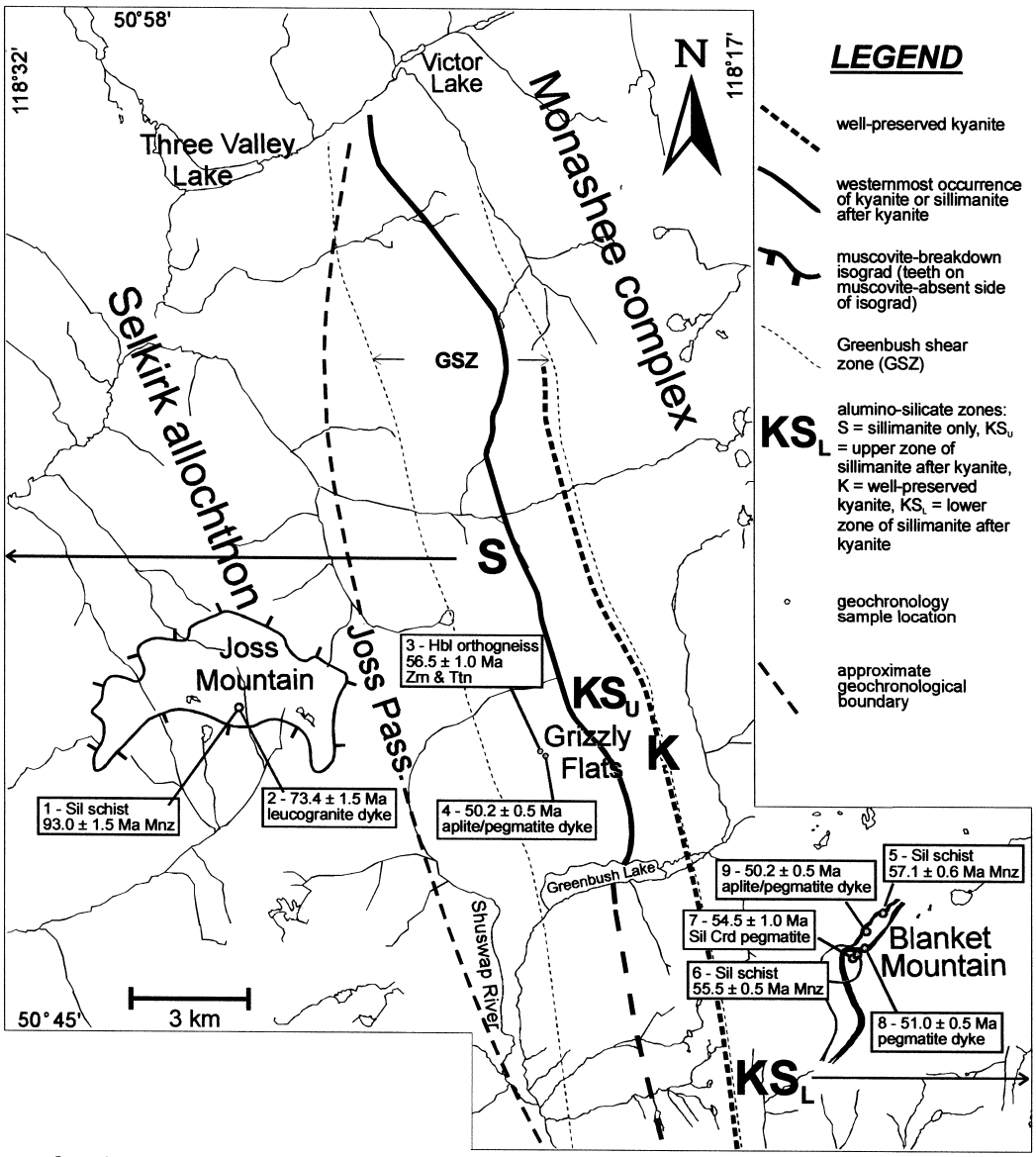

Sample	Mineral	Age (Ma)	Structural setting	Interpretation
Joss Mountain				
1 Sil schist	Mnz	93.0 ± 1.5		metamorphic or fluid related monazite growth at ~93 Ma
2 leucogranite	Mnz	73.4 ± 1.5	deformed by F_3	pegmatite is ~ 73 Ma & F_3 is younger than pegmatite
Grizzly Flats				
3 Hbl orthogneiss	Zrc, Ttn	56.5 ± 1.5	foliated	orthogneiss and/or anatexis is ~56.5 Ma, and foliation is, in part, ~56.5 Ma or younger
4 Tur aplite/peg	Mnz	50.2 ± 0.5	cross cuts all structures	D_1-D_5 is older than ~50 Ma
Blanket Mountain				
5 Sil schist	Mnz	57.1 ± 0.6		metamorphic or fluid related monazite growth at ~ 57 Ma
6 Sil schist	Mnz	55.5 ± 0.5		metamorphic or fluid related monazite growth at ~ 55.5 Ma
7 Sil pegmatite	Mnz	54.5 ± 1.0	infills F_1/F_2 boudin neck	Boudinage <54.5 Ma & F_3 - D_5 < 54.5 Ma
8 pegmatite	Zrc, Mnz	51.0 ± 0.5	cuts S_2 and F_3 folds	S_2 and F_3 are older than ~51 Ma
9 Tur aplite/peg	Mnz	50.2 ± 0.5	infills D_5 pull-apart	D_1 -D_5 are older than ~ 50 and D_5 occurred at ~ 50 Ma

Fig. 9. Map of the northwest Thor–Odin dome area showing the Greenbush shear zone, alumino-silicate zones and geochronological data.

isograd: Ms + Qtz = Kfs + Sil + melt (mineral abbreviations per Kretz, 1983; c.f. Johnson, 1994).

Coarse-grained minerals defining the regional foliation generally are recrystallized and show no evidence of strain or alteration that post-dates the peak of thermal metamorphism (e.g. sillimanite, sillimanite and/or biotite aggregates, elongate quartz grains). An important exception is in top-to-west-southwest D_5 shear bands, where minerals show abundant evidence of deformation and retrogression that post-dates the peak of thermal metamorphism; also L_5 pull-aparts are filled in with lower grade metamorphic minerals (e.g. muscovite, biotite and chlorite).

5.2. Westernmost occurrence of kyanite or sillimanite after kyanite; alumino-silicate zones

Fig. 9 shows the location of the westernmost occurrence of kyanite or kyanite that has been pseudomorphously replaced by sillimanite. Where kyanite is preserved, it occurs in an apparent equilibrium assemblage with biotite and garnet. Most of the kyanite has been pseudomorphously replaced by sillimanite. Four alumino-silicate zones can be delimited (Fig. 9). At deeper structural levels is a lower kyanite–sillimanite zone (KS_L) where kyanite has been pseudomorphously replaced by sillimanite. Above KS_L is a narrow discontinuous zone (K) where pristine blue kyanite is locally preserved. Above K is an upper kyanite–sillimanite zone (KS_U) in which kyanite is sporadically preserved but is predominately pseudomorphously replaced by sillimanite. West of KS_U, and extending into the Selkirk allochthon to the western limit of mapping and beyond (c.f. Johnson, 1994), there is no evidence of kyanite ever having been present (S zone, Fig. 9).

Along the west flank of the Thor–Odin dome, the westernmost occurrence of kyanite or kyanite that has been pseudomorphously replaced by sillimanite approximately parallels both the largest and the highest density of top-to-the-west-southwest D_5 extensional shear bands within the GSZ. Also, the K zone is approximately parallel to the base of the GSZ. These spatial relationships suggest that the preservation of relict kyanite is related to D_5 extension (i.e. rapid exhumation and cooling).

6. Geochronology

6.1. U–Pb geochronology

U–Pb zircon, monazite and titanite ages were determined (Fig. 9; Appendices A–C) for nine samples collected from lower structural levels of Thor–Odin dome (Blanket Mountain), higher levels of the dome (Grizzly Flats), and the overlying Selkirk allochthon (Joss Mountain). The zircons, with a few exceptions, are discordant due to inherited Pb, therefore, age determinations rely heavily on the monazite data.

Young monazites are commonly reversely discordant (i.e. $^{206}Pb/^{238}U$ dates > $^{207}Pb/^{235}U$ dates), and this is commonplace in samples from the Shuswap complex (Parrish, 1990; Carr, 1992; Scammell, 1993; Parrish, 1995; Digel et al., 1998; Crowley and Parrish, 1999; Appendices A and B). It is thought to be due to unsupported ^{206}Pb that resulted from incorporation of excess ^{230}Th during crystallization (Schärer, 1984; Parrish, 1990), therefore $^{207}Pb/^{235}U$ dates are reported here. Corrections for excess ^{206}Pb to the $^{206}Pb/^{238}U$ dates from intrusive rocks were not made using the method outlined by Schärer (1984) because Th/U whole rock ratios were not measured. As pointed out by Parrish (1990), there is little justification for the use of this correction on metamorphic monazite because it is impossible to determine the Th/U ratios of the fluids in which the mineral grew.

Diffusive Pb loss is ruled out in all analyses because many studies have shown that monazite is highly resistant to this thermally induced process (DeWolf et al., 1993; Zhu et al., 1997; Braun et al., 1998; Crowley and Ghent, 1999). However, we cannot rule out the possibility that the grains with reverse discordance underwent a minor amount of overgrowth or recrystallization, which commonly occurs in monazite (e.g. DeWolf et al., 1993; Poitrasson et al., 1996; Hawkins and Bowring, 1997; Braun et al., 1998; Crowley and Ghent, 1999). Concordant U–Pb dates are interpreted as growth or cooling ages, yet they could represent mixtures of primary domains with reverse discordance (due to excess ^{206}Pb) and secondary domains.

For both reversely discordant and concordant analyses, the replication of U–Pb dates is taken as an indication that the grains represent a single growth age rather than mixed ages because it is unlikely that numerous grains would contain identical mixtures of multiple age domains. When there is replication of three fractions, within error, we interpret the average age to represent the age of monazite growth. Errors are assigned on the basis of the range of ages and errors (e.g. the difference between youngest age minus its error and the oldest age plus its error divided by two).

6.2. Age interpretations

6.2.1. Joss Mountain

Sample 1 is from sillimanite–garnet–biotite–muscovite schist (Fig. 9). Monazites are xenoblastic, typically subrounded, and have numerous indentations. Three concordant or slightly normally discordant analyses have $^{207}Pb/^{235}U$ dates between 94.5 and 91.6 Ma (93.0 ± 1.5 Ma), and two reversely discordant analyses

are 89.9 ± 0.3 and 83.4 ± 0.3 Ma (Appendices Aa and B). The 93.0 ± 1.5 Ma cluster of dates is interpreted as closely representing a period of monazite growth. The two younger dates could be due to mixing of Late Cretaceous monazite and younger monazite, or they could be due to a protracted period of monazite growth, perhaps, in part, related to crystallization of leucogranite dykes that occur in the region (see sample 2, below). Monazite growth at 93.0 ± 1.5 Ma is taken to represent a regional metamorphic event; however, it may represent growth in response to a fluid influx.

Sample 2, collected a few metres from sample 1, is from a coarse-grained leucogranite dyke in the upper limb of a mesoscopic, shallowly south-southeast-plunging, F_3 fold (Fig. 7). Although it generally parallels S_2 in the host pelitic schist, apophyses are locally highly discordant to S_2. A weak foliation in the dyke is defined by the subparallel alignment of muscovite grains. Crystallization is interpreted as having predated F_3 folding because the weak foliation is interpreted as a refracted F_3 axial planar foliation.

Zircons are sharply faceted bipyramidal prisms with aspect ratios of 2:1 to 5:1. Morphology is consistent with an igneous origin; however, the grains have relatively low U concentrations relative to most zircons from leucogranites. A single-grain zircon analysis and two multigrain fractions yield discordant U–Pb analyses which plot near the concordia curve between 78 and 68 Ma (Appendices A, Fig. A1b, and Table B1). These data do not provide a reliable age. Monazites are xenoblastic to idioblastic. Three fractions yielded slightly reversely discordant $^{207}Pb/^{235}U$ dates between 74.9 ± 0.4 and 72.8 ± 0.8 Ma (Appendices A, Fig. A1b, and Table B1). The cluster of dates suggests that the grains are composed of monazite of a single age of 73.4 ± 1.5 Ma and is interpreted as representing the crystallization age of the dyke. This constrains the peak metamorphism and at least a portion of the development of S_2 to older than ~73 Ma and F_3 folding to a younger age.

6.2.2. Grizzly Flats

Sample 3 is from a coarse-grained 1 × 1.5-km body of hornblende-, plagioclase-, quartz- and K-feldspar-bearing orthogneiss with prominent K-feldspar augen. The foliation, defined by discontinuous ~1-mm-thick hornblende-rich and quartzo-feldspathic layers, is concordant with the locally reactivated S_2 foliation in the GSZ. Zircons are sharply faceted bipyramidal prisms with aspect ratios of 2:1–3:1, consistent with an igneous origin. Inclusions are common, and cores are not apparent. Five of the six zircon fractions yielded discordant U–Pb dates (Appendices A, Fig. A1c, d and Table B1). Analysis B has a higher U concentration (2511 ppm) and lower Th/U ratio (0.04) than the other fractions. It yielded a concordant analysis with a date of 56.5 ± 1.5 Ma, interpreted as the crystallization age of the zircon. Discordant fractions are interpreted as being Late Paleocene–Early Eocene zircons that contain components of inherited Proterozoic Pb (the lower and upper intersections of the discordia chords with the concordia curve, Appendix A, Fig. A1c).

Two fractions of tan-coloured disc-shaped titanite were dated. The $^{206}Pb/^{238}U$ dates are 57.7 ± 1.0 and 56.1 ± 0.8 Ma (Appendices A, Fig. A1d and Table B1). The $^{206}Pb/^{238}U$ dates are more reliable than the $^{207}Pb/^{235}U$ dates because they have a smaller uncertainty and smaller common Pb correction and, taken together with the relatively high closure temperature for Pb in titanite (e.g. Scott and St. Onge, 1996; Pidgeon et al., 1996), indicate that titanite growth occurred at 57.0 ± 2.0 Ma. Although it is not certain whether the growth of ca. 56.5 Ma zircon and titanite is a result of igneous crystallization or anatexis it is clear that the foliation in the rock is ~56.5 Ma or younger.

Sample 4 is from an undeformed tourmaline-bearing leucocratic dyke that truncates all structures and fabrics, including the west-dipping, west-southwest-directed D_5 shear bands. The dyke has an aplitic core bounded by pegmatitic margins, and has chilled contacts adjacent to the host psammo-pelitic gneiss. Monazites are colourless and euhedral to subhedral. Three single-grain, reversely discordant analyses have $^{207}Pb/^{235}U$ dates between 50.8 and 49.4 Ma (Appendices A, Fig. A1d and Table B1). The cluster of dates at 50.2 ± 0.5 Ma indicates that the grains are of a single age, which is interpreted as representing the igneous crystallization age of the dyke. This constrains the peak of metamorphism and F_1–D_5 to be older than ~50 Ma.

6.2.3. Blanket Mountain

Sample 5 is from migmatitic sillimanite biotite schist; some of the sillimanite appears to have replaced kyanite. The schist lies structurally above a quartzite inferred to be the basal unit of the cover sequence, and is interpreted as part of the cover sequence. Monazites are xenoblastic, typically subrounded, and have numerous indentations. Three single-grain, concordant analyses have $^{207}Pb/^{235}U$ dates that range from 57.6 to 56.4 Ma (Appendices A, Fig. A1e and Table B1). The small age range indicates that the grains comprise a single age (57.1 ± 0.6 Ma), which is taken as representing the age of monazite growth.

Sample 6 is from migmatitic sillimanite–biotite schist that lies structurally below the thick 'basal' quartzite, and is considered to be part of the basement (Fig. 2). Monazites are xenoblastic, typically subrounded, and have numerous indentations. Three single-grain analyses are concordant and overlap each other within

error; the $^{207}Pb/^{235}U$ dates range between 56.0 and 55.2 Ma (Appendices A, Fig. A1e and Table B1). This 55.5 ± 0.5 Ma date represents the age of monazite growth.

Sample 7 is from a sillimanite–cordierite pegmatite in the cover sequence that occurs in the neck of a boudin located on the limb of a F_1/F_2 fold. It is interpreted to have crystallized during F_1/F_2 or early F_3 folding. Some of the sillimanite appears to have pseudomorphously replaced kyanite. Monazites are clear and euhedral. Four single-grain, reversely discordant analyses have $^{207}Pb/^{235}U$ dates that range between 54.7 and 53.3 Ma (Appendices A, Fig. A1e and Table B1). The morphology and relatively high U concentrations indicate an igneous origin. The cluster indicates that the grains are composed of monazite of a single age of 54.5 ± 1.0 Ma. If this represents an igneous crystallization age then boudinage occurred after ca. 54.5 Ma, and the sillimanite overprint of kyanite is younger than ca. 54.5 Ma.

Samples 8 and 9 are from a tourmaline-bearing suite of dykes that occur in the Blanket Mountain area. Sample 8 is from an undeformed biotite, tourmaline, andalusite pegmatite dyke that cross-cuts east-trending, north-verging F_3 folds. Zircons are sharply faceted bipyramidal prisms with aspect ratios of 2:1–4:1, consistent with an igneous origin. Five single-grain zircon analyses are discordant and are interpreted as being Middle Eocene zircons that contain Proterozoic or older inherited Pb. Monazites are clear and euhedral. Three single-grain, reversely discordant analyses have 51.5–50.4 Ma $^{207}Pb/^{235}U$ dates (Appendices A, Fig A1f and Table B1). The tight range indicates that the grains are composed of monazite of a single age, taken to be 51.0 ± 0.5 Ma, which is the same, within error, as the lower intercept age of discordant zircon analyses (Appendices A, Fig. A1f and Table B1). The crystallization age of the pegmatite is interpreted as being 51.0 ± 0.5 Ma.

Sample 9 is from an undeformed tourmaline-bearing aplite to pegmatite dyke that intruded the Blanket megaboudin, has chilled margins and is interpreted as having infilled a D_5 pull-apart. Monazites are clear and euhedral, yield $^{207}Pb/^{235}U$ dates that range from 50.6 to 49.6 Ma (Appendices A, Fig. A1g and Table B1) and are taken to be 50.2 ± 0.5 Ma. Zircons from the aplite are small, cracked, have inclusions and are sharply faceted bipyramidal prisms with aspect ratios between 3 and 5. Zircon analyses are discordant due to inherited Pb. The monazite age of 50.2 ± 0.5 Ma is interpreted as the igneous crystallization age of the rock.

6.3. Conclusions

The U–Pb study shows that there is a difference in the ages of thermal and/or fluid history and intrusion of pegmatites at high structural levels at Joss Mountain (Selkirk Allochthon) relative to that of low and middle structural levels of Thor–Odin dome at Blanket Mountain and Grizzly Flats. Events at Joss Mountain are Late Cretaceous based on the 73.4 ± 1.5 Ma pegmatite and ~93 Ma monazites from a sillimanite schist (Samples 1 and 2, Fig. 9). At Grizzly Flats and Blanket Mountain (Fig. 9), monazites from schists are Eocene (55.5 and 57 Ma) as are deformed granitoids (54.5 and 56.5 Ma). Penetrative foliation development is as young as 56.5 Ma (sample 4) at Grizzly Flats. At Blanket Mountain, early F_3 may be as young as 54.5 Ma if monazite ages from the pegmatite in sample 7 represent an igneous crystallization age. The ~50 Ma age of the suite of late tourmaline-bearing pegmatites places an upper age bracket on F_1–F_4 and constrains the 50 Ma age of the D_5 extension event in the dome (Fig. 9). The geochronology data from the Thor–Odin dome are consistent with other studies from the region indicating that Shuswap complex rocks were deforming at high grade throughout the Paleocene and earliest Eocene, and were exhumed in an extensional setting in the Eocene (Parrish et al., 1988; Carr, 1992, 1995; Johnson, 1994; Johnson and Brown, 1996; Spear and Parrish, 1996; Simony and Carr, 1997; Crowley and Parrish, 1999).

7. Tectonic interpretation

7.1. Introduction

In the discussion that follows, we will argue that the structures and metamorphic minerals in crystalline rocks of the Monashee complex record northeastward ductile thrusting (F_1/F_2 and related fabrics; kyanite), extrusion (F_3, F_4; preserved kyanite) and exhumation (D_5; kyanite to sillimanite).

7.2. Discussion

Layer-parallel 'flow' or shear was top-to-the-northeast during F_1/F_2 deformation, as indicated by the deflection of metamorphic layers that were truncated at low angles to the transposition foliation as shear bands formed and by the asymmetry of most F_1/F_2 folds. The north- to northeast-trending L_{2i} lineation preserved at deep structural levels of the Thor–Odin dome is consistent with maximum stretch to the northeast. Pelitic schists at the lowest structural levels of the Thor–Odin dome are sillimanite- and K-feldspar-bearing, and there is no evidence of kyanite ever having been present (Spark, 1999; i.e. a 'S_L' zone at the lowermost structural level, southeast of the study area). This suggests that there is symmetry in the distribution of

the alumino-silicate zones (i.e. S_U, KS_U, K, KS_L, S_L). Development of the S_U–K–S_L symmetry, before most kyanite was pseudomorphously replaced by sillimanite, is best explained by northeastward thrusting of allochthonous rocks whereby relatively cool rocks, bounded above and below by relatively hot rocks, could be buried to deep crustal levels where kyanite could have formed (i.e. profile of isotherms mimic those of a subduction zone; Fig. 10). F_1/F_2 folds are overprinted by kyanite, suggesting that development of the transposition foliation may very well have begun during northeastward thrusting of the Selkirk allochthon above the North American basement and its sedimentary cover.

At deep structural levels of the Frenchman Cap dome, there are rocks interpreted as North American basement that are only weakly affected by Mesozoic to early Tertiary 'Cordilleran' metamorphism and deformation (Armstrong et al., 1991; Crowley, 1995, 1997b, 1999). Thus, there may be a lower limit to Cordilleran tectonism at deep structural levels of the Monashee complex, referred to here as the Cordilleran tectonic front (CTF).

With continued northeastward thrusting during the Mesozoic, eventually a gravitationally unstable crustal edifice formed (c.f. Coney and Harms, 1984; Brown and Journeay, 1987). Penetrative northeast-directed F_1/F_2 ductile flow within the large thickness of crystal-

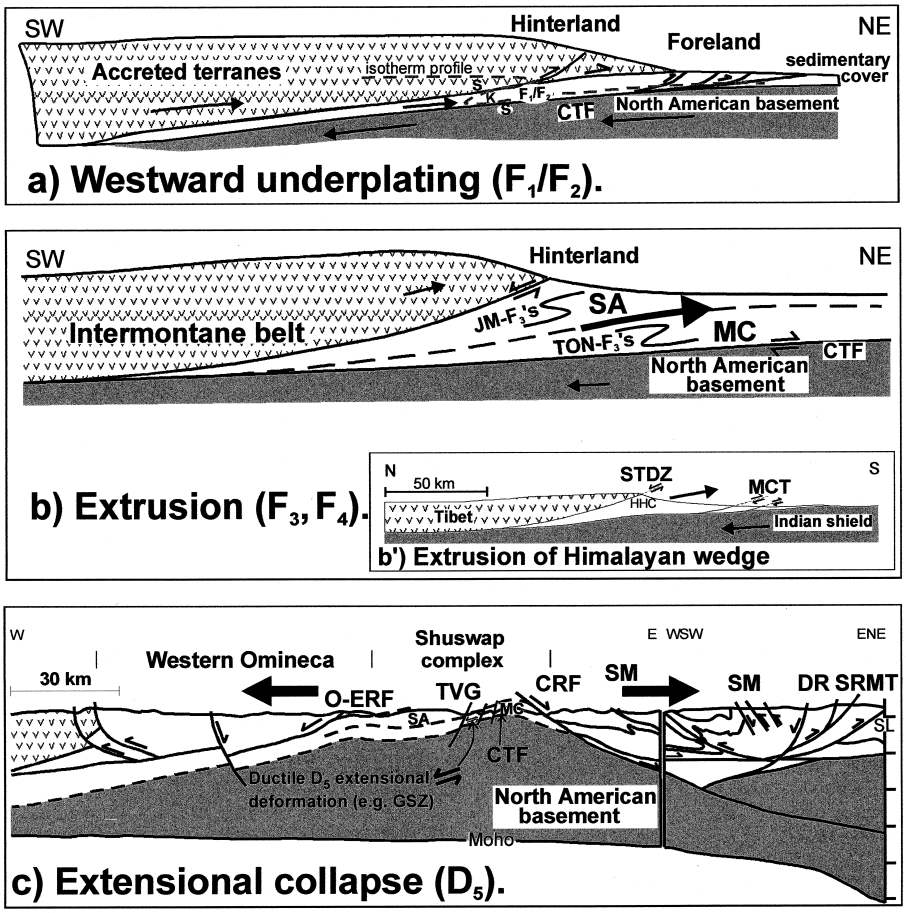

Fig. 10. Proposed tectonic evolution of the study area. Eastward subduction (not shown) is ongoing west of (a), (b) and (c). Horizontal and vertical scales equal in (b′) and (c). (a) Schematic cross-section, not to scale, showing F_1/F_2 northeast-directed flow of crystalline rocks of the Monashee complex above the Cordilleran tectonic front (CTF) during northeastward thrusting of hinterland rocks over North American basement and its sedimentary cover. S, sillimanite; K, kyanite. (b) Schematic cross-section, not to scale, relating major structures to extrusion of a crustal wedge between accreted terranes of the Intermontane belt and North American cratonic basement; wedge is interpreted as having been extruded in a manner similar to the Himalayan wedge shown in (b′). JM-F_3's, Joss Mountain F_3 folds; MC, Monashee complex; SA, Selkirk allochthon; TON-F_3's, Thor–Odin nappe F_3 folds (of Read and Klepacki, 1981). (b′) Schematic cross-section of the Himalayas showing extrusion of a crustal wedge between the STDZ (South Tibet detachment zone) and the MCT (Main Central Thrust) zone. HHC, High Himalaya Crystallines. From Grujic et al., 1996. (c) Extensional collapse of the southern Canadian Cordillera as shown in a crustal cross-section through the Omineca belt. The major faults interpreted from seismic data and surface geology are: O–ERF, Okanagan–Eagle River fault; MD, Monashee décollement; TVG, Three Valley Gap; CRF, Columbia River fault. SM, Selkirk Mountains, DR, Dogtooth Range; SRMT, Southern Rocky Mountain Trench; SL, sea level. Simplified from Johnson and Brown, 1996; modified only for the CTF and for the MC/SA contact since evidence of a MD was not observed. See text for discussion.

line rocks in the upper parts of the Monashee complex and the lower part of the Selkirk allochthon may have funnelled into discrete thrusts in the foreland. A complete analysis of the deformation of the hinterland of the southern Canadian Cordillera is beyond the scope of this paper and we will restrict our interpretation to the events that occurred as the unstable crustal edifice developed. The exact timing of this stage of crustal thickening is difficult to determine but based on the following it most probably occurred in the Late Cretaceous. The Monashee complex remained east of the magmatic front of the orogen until the Tertiary and there is no evidence of deep burial of the complex prior to this time. Geochronologic evidence indicates that the Monashee complex was rapidly exhumed in the Tertiary within a few millions of years of attaining peak metamorphic conditions (Parrish, 1995 and references therein). The lower part of the Selkirk allochthon did not attain high grade metamorphic conditions and was not migmatised or intruded by granitic plutons prior to the Late Cretaceous (Scammell, 1986; Carr, 1995; Parrish, 1995; Fig. 9). Accordingly we suggest that the F_1/F_2 deformation within the upper part of the Monashee complex and lower part of the Selkirk allochthon occurred in Late Cretaceous to Tertiary time. Approximately half of the shortening in the Rocky Mountain belt occurred at this time (Price and Mountjoy, 1970) and Rocky Mountain thrust faults presumably fed westward into the hinterland where the displacements were compensated by the northeasterly F_1/F_2 ductile flow.

Northeast-verging F_3 folds occur in the study area east of Joss Pass and throughout the Monashee complex (e.g. Journeay, 1986; Brown et al., 1992; McNicoll and Brown, 1995). Southwest-verging F_3 folds occur west of Joss Pass and throughout the remainder of the Shuswap complex (c.f. Jones, 1959; Carr, 1991; Scammell, 1993; Johnson, 1994). F_3 folds in both the Monashee complex and Selkirk allochthon are interpreted as having formed as dragfolds during the gravity-driven, northeastward extrusion of a crustal wedge from an overthickened, gravitationally unstable crustal edifice. Ductile extrusion occurred most rapidly in the middle of the wedge. Slower rates of ductile extrusion in the upper level of the Cordilleran wedge resulted in the formation of southwest-verging F_3 folds in the Selkirk allochthon (e.g. km-scale F_3 folds at Joss Mountain; Fig. 10b); slower rates in the lower levels of the wedge resulted in the formation of northeast-verging F_3 folds in the Monashee complex (e.g. km-scale F_3 folds of the Thor–Odin nappe of Read and Klepacki 1981; Fig. 10b). Temperatures continued to rise and/or pressures decreased as the rocks were extruded towards the earth's surface and eventually the rocks passed from the kyanite- to sillimanite-stable conditions. As the hot gneisses were brought to middle crustal levels, kyanite in KS_L and KS_U was pseudomorphously replaced by sillimanite. The preservation of kyanite (in the K zone) suggests that ductile extrusion of the gneisses occurred rapidly (c.f. Hill et al., 1992). North-northwest-trending F_4 folds are interpreted as representing layer-parallel shortening as ductile flow waned. Finally with the start of D_5, the rocks were brought more rapidly to the surface. D_5 continued and was in its final brittle stages by 51–52 Ma (as per the zircon and monazite ages of samples 8 and 9).

Extrusion of the Cordilleran wedge can be compared to the southward ductile extrusion of the High Himalaya Crystallines (Burchfiel et al., 1992 and references therein; Fig. 10b and b′). In both cases the extrusion occurred in an overall compressional setting during plate convergence and a period of crustal thickening. However, it is possible that in the Cordilleran orogenic wedge there was additional extrusion and foreland thrusting that occurred during gravity collapse; gravity collapse has not yet begun in the still-rising Himalayas.

The bounding structures of the Himalayan and Cordilleran wedges are comparable. In the Himalayas, the basal part of the wedge lies in the hanging wall of the south-directed Main Central Thrust and the upper part forms the footwall of the north-directed Southern Tibet detachment system. In the Cordillera, the basal part of the wedge is marked by a zone of northeast-directed ductile flow with an apparent decreasing downward gradient observed in the deep levels of Frenchman Cap dome (the Cordilleran tectonic front, CTF). This boundary lies within the Monashee complex and is not equivalent to the Monashee décollement as defined in the Frenchman Cap region (Brown et al., 1992 and references therein). The upper part of the wedge is marked by the presence of southwest-verging structures and at its highest level it lies in the footwall of the south-directed Okanagan–Eagle River detachment fault.

The final stages of extensional collapse of the southeastern Canadian Cordillera distinguishes it from the present status of the Himalayas (Fig. 10, c vs. b′). The rheological boundary between the extruded hot buoyant gneisses and cooler overlying rocks probably served as a locus for crustal-scale east- and west-dipping Eocene normal faults along which the crystalline rocks were exhumed (e.g. Okanagan–Eagle River fault, Columbia River fault; c.f. Parrish et al., 1988; Simony and Carr, 1997). Similarly, top-to-the-west-southwest extensional deformation within the D_5 Greenbush shear zone probably occurred where it did because overlying thick sheets of Joss Mountain orthogneiss (see Fig. 2) were cooler in the Eocene than underlying rocks of the Monashee complex. The strong L_5 lineation formed as relatively high temperatures persisted during D_5 top-to-the-west-southwest reactivated slip

on S_2. As temperatures decreased, L_5 pull-aparts formed and were infilled with low-grade minerals.

Normal displacement on the Three Valley–Joss Pass fault during brittle D_5 deformation obscures the reversal in tectonic vergence across Joss Pass. This fault and the larger normal faults that bounded the Shuswap and Monashee complexes, as well as top-to-the-west-southwest movement in the GSZ, are interpreted here as having formed in response to extensional stresses that developed as northeastward subduction slowed down beneath the southern Canadian Cordillera in the Eocene (Hyndman, 1995 and references therein).

8. Conclusions

An important implication of the model presented above is that exhumation of the large thicknesses of high-grade metamorphic rock of the Shuswap complex was the result of extrusion and extension, not extension alone, distinguishing the Shuswap complex from core complexes in the southwestern United States. Geochronological data presented in this paper indicate that rocks exposed in deep structural levels of the Shuswap complex (i.e. Monashee complex) were deforming at middle crustal depths when the youngest foreland thrusting was occurring (Early Eocene). However, our metamorphic and geochronological data allow the possibility that much of the early crustal thickening of the hinterland (F_1/F_2 deformation) may have occurred at low metamorphic grades at upper crustal levels and during this time hinterland thrusts may have fed directly into early foreland thrusts. Later thrusting in the foreland was accommodated in the hinterland, not by movement along a relatively discrete ductile thrust (i.e. along the Monashee décollement), but rather by the ductile flow of large thicknesses of middle crustal rocks during the later stages of crustal thickening (F_1/F_2), extrusion (F_3 and F_4) and extension (D_5).

Price and Mountjoy (1970) correlated the ductile flow of gneisses in the hinterland with foreland thrusting. More recently, Vanderhaeghe and Teyssier (1997) proposed that the domal culminations of the Monashee complex are the result of upwelling Eocene migmatites that triggered late-orogenic gravitational collapse of the hinterland; they link this gravitational collapse with coeval foreland thrusting. The problem with diapiric models such as these is that they cannot be reconciled with rocks interpreted as North American basement that occur at deep structural levels of the Frenchman Cap dome and that are only weakly affected by Mesozoic to early Tertiary 'Cordilleran' metamorphism and deformation.

Geochronological data indicate that much of the Monashee complex was affected by significant Cordilleran metamorphism and deformation, but only during Paleogene time (60–55 Ma, Parrish, 1995; this study). This strongly suggests that the Monashee complex remained a basement high until very late in the history of the Cordilleran orogen before it was brought to middle crustal levels and rapidly exhumed. Because of this limited time frame (i.e. 60–55 Ma), we believe that extrusion and ductile extensional deformation, rather than brittle–ductile to brittle extensional deformation, were primarily responsible for the rapid exhumation of the Monashee complex.

Acknowledgements

This paper is based on research for D.H. Johnston's Ph.D. thesis, research at Blanket Mountain by P.F. Williams and regional studies by R. L. Brown. The research was funded by a National Science and Engineering Research Council (NSERC) grants to P.F. Williams and R.L. Brown. Geochronology was carried out by J.L. Crowley in S. Carr's geochronology lab at Carleton University; we appreciate the support of John Blenkinsop in mass spectrometry and data reduction. Vicki McNicoll at the Geochronology Laboratory in Ottawa provided U–Pb data for one sample. We thank reviewers James Hibbard and Don Fisher for their constructive criticism and recommended revisions. H.D. Gibson and R.R. Parrish are thanked for vigorous discussions of Monashee complexities. Duncan Wassick is thanked for very capable helicopter flying.

Appendix A. U–Pb concordia plots

In Fig. A1, ellipses for the analyses represent the two sigma uncertainty (95% confidence level) and analyses that are plotted with + symbols have ellipses that are too small to be seen at this scale. Monazite analyses are identified with numbers and zircon analyses are identified with letters. See Appendix B for analytical data. Mineral abbreviations after Kretz (1983).

Appendix B. U–Pb analytical data (Table B1)

Appendix C. U–Pb geochronology: analytical methods

U–Pb geochronology including the measurement of isotropic ratios on a MAT 261 mass spectrometer was carried out in the laboratories at Carleton University, although some mass spectrometry was done at the Geological Survey of Canada (GSC) in Ottawa, and

Vicki McNicoll of the GSC provided some of the data for sample 2 (sample VM). U–Pb IDTIMS geochronology followed the procedure outlined by Parrish et al. (1987) using microcapsules for mineral dissolution (Parrish, 1987), a mixed ^{233}U–^{235}U–^{205}Pb tracer (Parrish and Krogh, 1987), multicollector mass spectrometry (Roddick et al., 1987), and estimation of errors using numerical error propagation (Roddick, 1987). Decay constants used are those recommended by Steiger and Jäger (1977). Discordia chords through analyses were calculated with the use of a modified York (1969) regression (Parrish et al., 1987), which

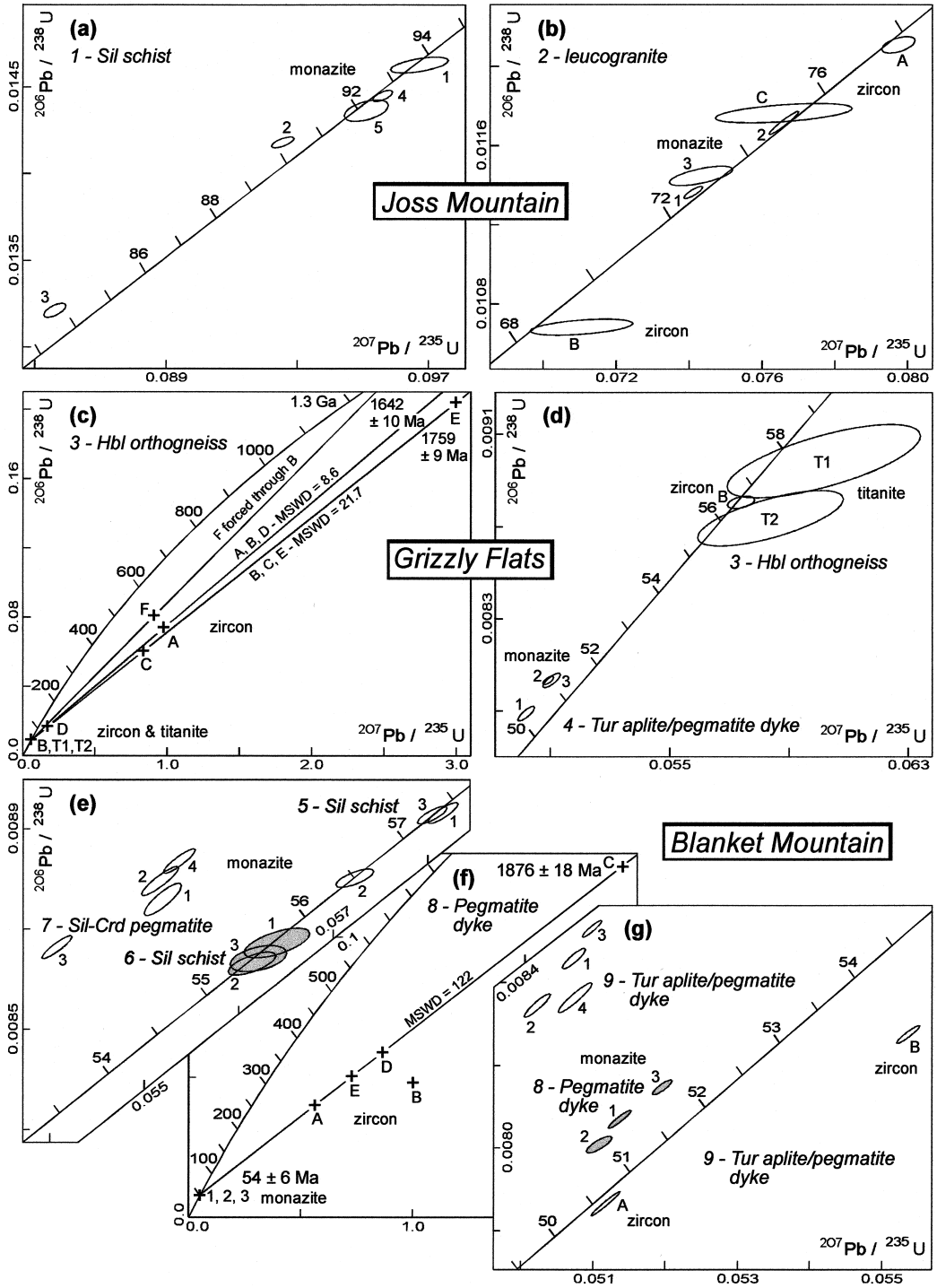

Fig. A1. U–Pb concordia plots.

Table B1
U–Pb analytical data[a]

Analysis[b]	Weight (μg)[c]	U (ppm)	Pb (ppm)[d,e]	$^{206}Pb/^{204}Pb$[f]	Pb_c (pg)[g]	^{208}Pb (%)[h]	$^{206}Pb/^{238}U$[i]	$^{207}Pb/^{235}U$[i]	$^{207}Pb/^{235}U$ age (Ma)[j]	Correlation coeffient	$^{207}Pb/^{206}Pb$[i]	$^{207}Pb/^{206}Pb$ age (Ma)[j]
Sample 1 (S279-160) Appendix Ia; sillimanite schist, Joss Mountain; 397400E, 5630690N.												
1	1,105	7	3306	122.7	440	51	64.3	0.014626±0.16%	0.09672±0.45%	93.7±0.8	0.58	0.04796±0.38%	97.3±18.2
2	1,105	8	4645	155.2	2042	17	61.6	0.014182±0.11%	0.09256±0.18%	89.9±0.3	0.70	0.04734±0.13%	66.3±6.4
3	1,105	9	4313	132.8	3036	11	61.2	0.013213±0.15%	0.08560±0.20%	83.4±0.3	0.65	0.04699±0.15%	48.6±7.3
4	1,105	7	5061	231.2	3372	9	71.3	0.014449±0.11%	0.09560±0.16%	92.7±0.3	0.67	0.04799±0.12%	98.7±5.6
5	1,105	2	8318	425.0	1218	13	74.5	0.014364±0.21%	0.09511±0.35%	92.2±0.6	0.49	0.04802±0.31%	100.4±14.7
Sample 2 (S279-40) Appendix Ib; leucogranite dyke, Joss Mountain; 397400E, 5630690N.												
A	1,149	27	494.3	5.677	1048	10	5.0	0.012108±0.17%	0.07975±0.29%	77.9±0.4	0.53	0.04777±0.25%	87.9±11.7
B	2,105	19	174.5	1.758	377	6	4.4	0.010683±0.19%	0.07105±0.99%	69.7±1.3	0.47	0.04824±0.91%	110.8±43.2
C	3,105	13	196.1	2.307	286	7	9.9	0.011764±0.21%	0.07660±1.20%	74.9±1.8	0.49	0.04723±1.10%	60.7±54.2
1	1,149	13	4385	163.1	1897	21	72.3	0.011363±0.13%	0.07411±0.17%	72.6±0.2	0.86	0.04730±0.09%	64.5±4.3
2	2,149	11	12 782	239.4	2200	47	43.5	0.011715±0.25%	0.07660±0.27%	74.9±0.4	0.96	0.04743±0.08%	70.7±3.6
3	2,149	14	1363	133.0	332	43	89.4	0.011447±0.21%	0.07433±0.58%	72.8±0.8	0.66	0.04710±0.47%	54.0±22.5
Sample 3 (S279-151) Appendix Ic,d; hornblende orthogneiss, Grizzly Flats; 404560E, 5629670N.												
A	1,149	19	158.9	13.97	2169	6	20.7	0.073814±0.11%	0.97742±0.14%	692.3±1.4	0.77	0.09604±0.09%	1548.5±3.4
B	1,105	8	2511	20.18	974	12	1.3	0.008806±0.15%	0.05738±0.40%	56.7±0.4	0.43	0.04726±0.36%	62.4±17.1
C	1,105	10	513	34.39	2599	7	14.9	0.060236±0.12%	0.83518±0.14%	616.5±1.3	0.85	0.10056±0.07%	1634.4±2.7
D	1,105	6	963	15.60	118	60	2.4	0.017135±0.49%	0.17107±1.10%	160.3±3.3	0.66	0.07241±0.86%	997.4±34.8
E	1,105	5	450	89.74	3388	8	2.6	0.204056±0.11%	2.99539±0.12%	1406.4±1.8	0.82	0.10646±0.07%	1739.7±2.5
F	1,105	4	268	22.81	164	33	11.7	0.080855±0.26%	0.90818±0.88%	656.1±8.5	0.62	0.08146±0.75%	1232.6±29.4
T1	20,149	377	217.6	2.199	80	766	19.7	0.008984±0.88%	0.06016±2.7%	59.3±3.1	0.69	0.04857±2.2%	127.0±102.9
T2	47,149	541	227.0	2.200	98	863	18.7	0.008737±0.69%	0.05837±2.1%	57.6±2.3	0.69	0.04846±1.7%	121.7±79.8
Sample 4 (S279-150) Appendix Id; tourmaline aplite/pegmatite dyke, Grizzly Flats; 404610E, 5629610N.												
1	1,149	15	21 992	270.0	1005	170	42.0	0.007888±0.20%	0.05020±0.28%	49.7±0.3	0.83	0.04615±0.16%	5.6±7.6
2	1,149	10	17 010	255.1	1335	66	51.6	0.008032±0.11%	0.05093±0.18%	50.4±0.2	0.73	0.04599±0.12%	−3.1±5.8
3	1,149	22	18 411	240.1	917	227	44.4	0.008032±0.20%	0.05104±0.29%	50.5±0.3	0.80	0.04609±0.18%	2.2±8.5
Sample 5 (S279-155) Appendix Ie; sillimanite schist, Blanket Mountain, 412780E, 5625760W.												
1	1,149	27	6311	142.8	3780	26	64.2	0.008932±0.12%	0.05816±0.14%	57.4±0.2	0.86	0.04722±0.07%	60.5±3.3
2	1,149	15	6817	156.5	1303	45	65.3	0.008803±0.10%	0.05723±0.18%	56.5±0.2	0.73	0.04715±0.12%	56.9±5.8
3	1,149	14	7058	144.0	3916	15	60.4	0.008928±0.10%	0.05805±0.13%	57.3±0.1	0.81	0.04715±0.08%	56.9±3.8
Sample 6 (S279-152) Appendix Ie; sillimanite schist, Blanket Mountain, 412120E, 5624610N.												
1	1,105	4	12 768	264.3	764	38	62.1	0.008673±0.17%	0.05640±0.31%	55.7±0.3	0.64	0.04717±0.24%	57.8±11.4
2	1,105	5	14 947	348.9	1001	42	66.5	0.008632±0.13%	0.05614±0.22%	55.5±0.2	0.68	0.04717±0.17%	57.9±7.9
3	1,105	5	8674	251.9	1118	20	73.0	0.008642±0.15%	0.05621±0.27%	55.5±0.3	0.43	0.04717±0.24%	58.0±11.6
Sample 7 (RB-1-93) Appendix Ie; sillimanite-cordierite pegmatite, Blanket Mountain, 411760E, 5624810N.												
1	1,149	22	15 907	282.5	4977	39	55.4	0.008760±0.19%	0.05520±0.18%	54.6±0.2	0.86	0.04570±0.10%	−18.2±4.7
2	1,149	13	13 640	273.3	3700	26	60.3	0.008796±0.16%	0.05517±0.18%	54.5±0.2	0.90	0.04548±0.08%	−29.6±3.7

(continued on next page)

Table B1 (*continued*)

Analysis[b]	Weight (μg)[c]	U (ppm)	Pb (ppm)[d,e]	$^{206}Pb/^{204}Pb$[f]	Pb_c (pg)[g]	^{208}Pb (%)[h]	$^{206}Pb/^{238}U$[i]	$^{207}Pb/^{235}U$[i]	$^{207}Pb/^{235}U$ age (Ma)[j]	Correlation coeffient	$^{207}Pb/^{206}Pb$[i]	$^{207}Pb/^{206}Pb$ age (Ma)[j]
3	1,149	24	12 222	218.9	5063	32	56.3	0.008664±0.13%	0.05407±0.15%	53.5±0.2	0.91	0.04526±0.06%	−41.5±3.0
4	1,149	28	11 819	238.7	4404	42	60.5	0.008836±0.14%	0.05537±0.15%	54.7±0.2	0.90	0.04545±0.07%	31.6±3.2
Sample 8 (S279-153) Appendix If,g; pegmatite dyke, Blanket Mountain, 412252E, 5624711N.													
A	1,149	13	1219	53.94	6341	6	14.1	0.040054±0.10%	0.56322±0.11%	453.6±0.8	0.93	0.10198±0.04%	1660.5±1.5
B	1,149	16	1404	84.01	14 161	5	20.0	0.048330±0.09%	1.00024±0.10%	703.9±1.0	0.95	0.15010±0.03%	2347.1±1.1
C	1,149	15	595.1	142.8	10 956	7	49.8	0.125570±0.09%	1.93580±0.10%	1093.5±1.3	0.93	0.11181±0.04%	1829.0±1.3
D	1,105	9	872.0	51.56	4276	7	5.6	0.058637±0.10%	0.86521±0.12%	633.0±1.1	0.92	0.10702±0.05%	1749.2±1.7
E	1,105	8	1948	101.6	5885	8	7.7	0.050685±0.10%	0.73011±0.11%	556.6±0.9	0.93	0.10447±0.04%	1705.1±1.5
1	1,149	33	9643	161.3	4088	40	56.4	0.008071±0.13%	0.05137±0.15%	50.9±0.2	0.94	0.04616±0.05%	5.8±2.5
2	1,149	17	10 882	179.6	1590	60	56.1	0.008010±0.12%	0.05109±0.17%	50.6±0.2	0.81	0.04626±0.10%	11.0±4.9
3	1,149	18	10 141	176.5	4638	20	57.7	0.008148±0.11%	0.05196±0.13%	51.4±0.2	0.87	0.04625±0.06%	10.5±3.1
Sample 9 (RB-2-93 and VM) Appendix Ig; tourmaline aplite/pegmatite dyke, Blanket Mountain; 412600E, 5625330N.													
A[d]	66,74	30	18 658	132.3	9759	29	0.2	0.007867±0.19%	0.05117±0.19%	50.7±0.2	0.98	0.04718±0.04%	58.3±0.9
B[d]	77,74	13	15 114	116.5	4241	25	3.3	0.008274±0.13%	0.05537±0.15%	54.7±0.2	0.94	0.04853±0.05%	125.3±2.4
1	1,149	18	19 646	252.7	5845	32	40.8	0.008460±0.15%	0.05073±0.16%	50.2±0.2	0.89	0.04349±0.07%	−139.5±3.5
2	1,149	12	22 633	282.2	5411	27	39.7	0.008346±0.17%	0.05022±0.18%	49.8±0.2	0.92	0.04364±0.07%	−130.7±3.4
3[d]	1,149	83	13 200	220.5	5604	103	54.0	0.008533±0.12%	0.05100±0.14%	50.5±0.1	0.94	0.04335±0.05%	−147.7±2.5
4[d]	4,105	22	28 659	345.2	4647	70	37.5	0.008364±0.22%	0.05075±0.23%	50.3±0.2	0.94	0.04401±0.08%	−110.3±4.0

[a] Isotopic composition of Carleton University laboratory blank (uncertainty is one standard deviation): 206:207:208:204 = 19.01±0.36:15.64±0.20:38.23±0.74:1.

[b] A–F = fraction codes for zircon analyses; 1–5 = fraction codes for monazite analyses; T1–2 = fraction codes for titanite analyses.

[c] Weights were estimated from grain size measurements; uncertainty is 2 μg.

[d] * = chemistry performed at the Geological Survey of Canada (all other chemistry performed at Carleton University); 1–42 in second column = number of grains analysed; 105, 149 = average size in μm.

[e] Radiogenic Pb.

[f] Measured ratio, corrected for spike and Pb fractionation of 0.09±0.03%/a.m.u.

[g] Total common Pb in analysis, corrected for spike and fractionation.

[h] Radiogenic ^{208}Pb, expressed as percentage of total radiogenic Pb.

[i] Corrected for blank Pb and U and common Pb (Stacey–Kramers model Pb composition equivalent to the interpreted age of the analyses); errors are one standard deviation in percent.

[j] Errors are two standard deviations in Ma.

takes scatter into account. For zircon and monazite chemistry, U blanks were less than 5 pg and Pb blanks were usually 5–20 pg. For titanite chemistry, U blanks were less than 5 pg and Pb blanks were ~20 pg.

The clearest and least magnetic zircons with the fewest inclusions and cracks were analysed. All analysed zircons were abraded (Krogh, 1982). The clearest monazites and titanites with the fewest inclusions were analysed. Grains that contain xenocrystic cores visible with a microscope in transmitted light were avoided.

References

Armstrong, R.L., Parrish, R.R., van der Heyden, P., Scott, K., Runkle, D., Brown, R.L., 1991. Early Proterozoic basement exposures in the southern Canadian Cordillera: core gneiss of the Frenchman Cap, Unit I of the Grand Fork Gneiss, and the Vaseaux Formation. Canadian Journal of Earth Sciences 28, 1169–1201.

Bell, T.H., Etheridge, M.A., 1973. Microstructure of mylonites and descriptive terminolgy. Lithos 6, 337–348.

Berthé, D., Choukroune, P., Jegouzo, P., 1979. Orthogneiss, mylonite and non-coaxial deformation of granites: the example of the South Armoricain shear zone. Journal of Structural Geology 1, 31–42.

Braun, I., Montel, J.M., Nicollet, C., 1998. Electron microprobe dating of monazites from high-grade gneisses and pegmatites of the Kerala Khondalite Belt, southern India. Chemical Geology 146, 65–85.

Brown, R.L., 1980. Frenchman Cap dome, Shuswap Complex, British Columbia: a progress report. In: Current Research, Part A. Geological Survey of Canada, Paper 80-1A, pp. 47–51.

Brown, R.L., Journeay, J.M., 1987. Tectonic denudation of the Shuswap metamorphic terrane of southeastern British Columbia. Geology 15, 142–146.

Brown, R.L., Journeay, M., Lane, L.S., Murphy, D.C., Rees, C.J., 1986. Obduction, backfolding and piggyback thrusting in the metamorphic hinterland of the southeastern Canadian Cordillera. Journal of Structural Geology 8, 255–268.

Brown, R.L., Carr, S.D., Johnson, B.J., Coleman, V.J., Cook, F.A., Varsek, J.L. 1992. The Monashee décollement of the southern Canadian Cordillera: a crustal-scale shear zone linking the Rocky Mountain foreland belt to lower crust beneath accreted terranes. In: McClay, K.R. (Ed.), Thrust tectonics. Chapman & Hall, London, pp. 357–364.

Burchfiel, B.C., Chen, Z., Hodges, K.V., Liu, Y., Royden, L.H., Deng, C., Xu, J., 1992. The South Tibetan Detachment system: Extension contemporaneous with and parallel to shortening in a collisional mountain belt. Geological Society of America, Special Paper 269, 41 pp.

Carr, S.D., 1991. Three crustal zones in the Thor–Odin–Pinnacles area, southern Omineca Belt, British Columbia. Canadian Journal of Earth Sciences 28, 2003–2023.

Carr, S.D., 1992. Tectonic setting and U–Pb geochronology of the early Tertiary Ladybird leucogranite suite, Thor–Odin–Pinnacles area, southern Omineca Belt, British Columbia. Tectonics 11, 258–278.

Carr, S.D., 1995. The southern Omineca belt, British Columbia: new perspectives from the Lithoprobe Geoscience Program. Canadian Journal of Earth Sciences 32, 1720–1739.

Cook, F.A., Varsek, J.L., Clowes, R.M., Kanasewich, E.R., Spencer, C.S., Parrish, R.R., Brown, R.L., Carr, S.D., Johnson, B.J., Price, R.A., 1992. LITHOPROBE crustal reflection cross-section of the southern Canadian Cordillera, 1. Foreland thrust and Fold Belt to Fraser River Fault. Tectonics 11, 12–35.

Cook, F.A., 1995. Lithospheric processes and products in the southern Canadian Cordillera: a Lithoprobe perspective. Canadian Journal of Earth Sciences 32, 1803–1824.

Coney, P.J., Harms, T.A., 1984. Cordilleran metamorphic core complexes: Cenozoic extensional relics of Mesozoic compression. Geology 12, 550–554.

Craig, D.B., 1966. Structure and petrology within the Shuswap metamorphic complex, Revelstoke, British Columbia. Ph.D. thesis, University of Wisconsin.

Crowley, J.L., 1995. Geochronological constraints on Early Proterozoic tectonism and Cordilleran overprinting in the Monashee complex, British Columbia. Geological Association of Canada/Mineralogical Association of Canada, Abstracts with Program 20, A-21.

Crowley, J.L., 1997a. U–Pb geochronologic constraints on the cover sequence of the Monashee complex, Canadian Cordillera: Paleoproterozoic deposition on basement. Canadian Journal of Earth Sciences 34, 1008–1022.

Crowley, J.L., 1997b. U–Pb geochronology in Frenchman Cap dome of the Monashee complex, southern Canadian Cordillera: early Tertiary overprint of a Proterozoic history. Ph.D. thesis, Carleton University.

Crowley, J.L., 1999. U–Pb geochronologic constraints on Paleoproterozoic tectonism in the Monashee complex, Canadian Cordillera: elucidating an overprinted geologic history. Geological Society of America Bulletin 111, 560–577.

Crowley, J.L., Ghent, E.D., 1999. An electron microprobe study of the U–Th–Pb systematics of metamorphosed monazite: the role of Pb diffusion versus overgrowth and recrystallization. Chemical Geology 157, 285–302.

Crowley, J.L., Parrish, R.R., 1999. U–Pb isotopic constraints on diachronous metamorphism of variable intensity in the northern Monashee complex, southern Canadian Cordillera. Journal of Metamorphic Geology 17, 483–502.

DeWolf, C.P., Belshaw, N., O'Nions, R.K., 1993. A metamorphic history from micron-scale $^{207}Pb/^{206}Pb$ chronometry of Archean monazite. Earth and Planetary Science Letters 120, 207–220.

Digel, S.G., Ghent, E.D., Carr, S.D., Simony, P.S., 1998. Early Cretaceous kyanite–sillimanite metamorphism and Paleocene sillimanite overprint near Mount Cheadle, southeastern British Columbia: geometry, geochronology, and metamorphic interpretations. Canadian Journal of Earth Sciences 35, 1070–1087.

Duncan, I.J., 1984. Structural evolution of the Thor–Odin gneiss dome. Tectonophysics 101, 87–130.

Gabrielse, H., Yorath, C.J., 1991. Tectonic synthesis, Chapter 18. In: Gabrielse, H., Yorath, C.J. (Eds.), Geology of the Cordilleran Orogen in Canada. Geological Survey of Canada, Geology of Canada, no. 4, pp. 677–705.

Grujic, D., Casey, M., Davidson, C., Hollister, L.S., Kündig, R., Pavlis, T., Schmid, S., 1996. Ductile extrusion of the Higher Himalaya Crystalline in Bhutan: evidence from quartz microfabrics. Tectonophysics 260, 21–43.

Hawkins, D.P., Bowring, S.A., 1997. U–Pb systematics of monazite and xenotime: case studies from the Paleoproterozoic of the Grand Canyon, Arizona. Contributions to Mineralogy and Petrology 127, 87–103.

Hill, E.J., Baldwin, S.L., Lister, G.S., 1992. Unroofing of active metamorphic core complexes in the D'Entrecasteaux Islands, Papua New Guinea. Geology 20, 907–910.

Hobbs, B.E., Means, W.D., Williams, P.F., 1976. An Outline of Structural Geology. Wiley, New York.

Hyndman, R.D., 1995. The lithoprobe corridor across the Vancouver Island continental margin: the structural and tectonic consequences of subduction. Canadian Journal of Earth Sciences 32, 1777–1802.

Johnson, B.J., 1994. Structure and tectonic setting of the Okanagan Valley fault system in the Shuswap Lake area, southern British Columbia. Ph.D. thesis, Carleton University.

Johnson, B.J., Brown, R.L., 1996. Crustal structure and early Tertiary extensional tectonics of the Omineca belt at 51°N latitude, southern Canadian Cordillera. Canadian Journal of Earth Sciences 33, 1596–1611.

Jones, A.G., 1959. Vernon map-area, British Columbia. Geological Survey of Canada, Memoir 296.

Journeay, J.M., 1986. Stratigraphy, internal strain and thermo-tectonic evolution of the northern Frenchman Cap dome: an exhumed duplex structure, Omineca hinterland, southeastern Canadian Cordillera. Ph.D. thesis, Queen's University.

Journeay, J.M., Brown, R.L., 1986. Major tectonic boundaries of the Omineca belt in southern British Columbia: a progress report. In: Current research, Part A. Geological Survey of Canada, Paper 86-1A, pp.81–88.

Kretz, R., 1983. Symbols for rock-forming minerals. American Mineralogist 68, 277–279.

Krogh, T.E., 1982. Improved accuracy of U–Pb zircon ages by the creation of more concordant systems using an air abrasion technique. Geochimica et Cosmochimica Acta 46, 637–649.

Lane, L.S., Ghent, E.D., Stout, M.Z., Brown, R.L., 1989. *P–T* history and kinematics of the Monashee décollement near Revelstoke, British Columbia. Canadian Journal of Earth Sciences 26, 231–243.

Lister, G.S., Snoke, A.W., 1984. *S–C* mylonites. Journal of Structural Geology 6, 617–638.

Mawer, C.K., Williams, P.F., 1991. Progressive folding and foliation development in a sheared coticule-bearing pyllite. Journal of Structural Geology 13, 539–555.

McMillan, W.J., 1973. Petrology and structure of the west flank, Frenchman Cap dome, near Revelstoke, British Columbia, Geological Survey of Canada, Paper 71-29.

McNicoll, V.J., Brown, R.L., 1995. The Monashee décollement at Cariboo Alp, southern flank of the Monashee complex, southern British Columbia, Canada. Journal of Structural Geology 17, 17–30.

Monger, J.W.H., Berg, H.C., 1984. Lithotectonic terrane map of western Canada and southeastern Alaska. In: Silberling, N.J., Jones D.L. (Eds.), Lithotectonic terrane maps of the North American Cordillera. U.S. Geological Survey Open File Report 84-523.

Monger, J.W.H., Price, R.A., Templeman-Kluit, D., 1982. Tectonic accretion and the origin of two major metamorphic and plutonic welts in the Canadian Cordillera. Geology 10, 70–75.

Parkinson, D.L., 1991. Age and isotropic character of early Proterozoic basement gneisses in the southern Monashee complex, southeastern British Columbia. Canadian Journal of Earth Sciences 28, 1159–1168.

Parrish, R.R., 1987. An improved microcapsule for zircon dissolution in U–Pb geochronology. Chemical Geology (Isotope Geoscience Section) 66, 99–102.

Parrish, R.R., 1990. U–Pb dating of monazite and its applications to geological problems. Canadian Journal of Earth Sciences 27, 1431–1450.

Parrish, R.R., 1995. Thermal evolution of the southern Canadian Cordillera. Canadian Journal of Earth Sciences 32, 1618–1642.

Parrish, R.R., Krogh, T.E., 1987. Synthesis and purification of ^{205}Pb for U–Pb geochronology. Chemical Geology (Isotope Geoscience Section) 66, 103–110.

Parrish, R.R., Roddick, J.C., Loveridge, W.D., Sullivan, R.W., 1987. Uranium–lead analytical techniques at the Geochronology Laboratory. In: Radiogenic age and isotopic studies, Report 1. Geological Survey of Canada, Paper 872, pp. 3–7.

Parrish, R.R., Carr, S.D., Parkinson, D.L., 1988. Eocene extensional tectonics and geochronology of the southern Omineca Belt, British Columbia and Washington. Tectonics 7, 181–212.

Pidgeon, R.T., Bosch, D., Bruguier, O., 1996. Inherited zircon and titanite U–Pb systems in an Archaean syenite from southwestern Australia: implications for U–Pb stability of titanite. Earth and Planetary Science Letters 141, 187–198.

Poitrasson, F., Chenery, S., Bland, D.J., 1996. Contrasted monazite hydrothermal alteration mechanisms and their geochemical implications. Earth and Planetary Science Letters 145, 79–96.

Price, R.A., Mountjoy, E.W., 1970. Geologic structure of the Canadian Rocky Mountains between Bow and Athabasca Rivers—a progress report. In: Wheeler, J.O. (Ed.), Structure of the southern Canadian Cordillera, Geological Association of Canada, Special Paper 6, pp. 7–25.

Read, P.B., 1980. Stratigraphy and structure: Thor–Odin to Frenchman Cap "domes", Vernon east-half map area, southern British Columbia. In: Current research, Part A. Geological Society of Canada, Paper 80-1A, pp. 19–25.

Read, P.B., Brown, R.L., 1981. Columbia River fault zone: southeastern margin of the Shuswap and Monashee complexes, southern British Columbia. Canadian Journal of Earth Sciences 18, 1127–1145.

Read, P.B., Klepacki, D.W., 1981. Stratigraphy and structure: northern half of Thor–Odin Nappe, Vernon east-half map area, southern British Columbia. In: Current research, Part A. Geological Society of Canada, Paper 81-1A, pp. 169–173.

Roddick, J.C., 1987. Generalized numerical error analysis with applications to geochronology and thermodynamics. Geochimica et Cosmochimica Acta 51, 2129–2135.

Roddick, J.C., Loveridge, W.D., Parrish, R.R., 1987. Precise U/Pb dating of zircon at the subnanogram Pb level. Chemical Geology (Isotope Geoscience Section) 66, 111–121.

Sander, B., 1911. Über Zusammenhange Zwischen Teilbewegung und Gefüge in Gesteinen. Tschermaks Mineral. Petrogr. Mitt. 30, 381–384.

Scammell, R.J., 1986. Stratigraphy, structure and metamorphism of the north flank of the Monashee complex, southeastern British Columbia: A record of Proterozoic extension and Phanerozoic crustal thickening. M.Sc. thesis, Carleton University.

Scammell, R.J., 1993. Mid-Cretaceous to Tertiary thermotectonic history of former mid-crustal rocks, southern Omineca Belt, Canadian Cordillera. Ph.D. thesis, Queen's University.

Scammell, R.J., Brown, R.L., 1990. Cover gneisses of the Monashee terrane: a record of synsedimentary rifting in the North American Cordillera. Canadian Journal of Earth Sciences 27, 712–726.

Schärer, U., 1984. The effect of initial ^{230}Th disequilibrium on young U–Pb ages: the Makalu case, Himalaya. Earth and Planetary Science Letters 67, 191–204.

Scott, D.J., St. Onge, M.R., 1996. Constraints on Pb closure temperatures in titanite based on rocks from the Ungave orogen, Canada: Implications for U–Pb geochronology and P–T–t path determinations. Geology 23, 1123–1126.

Simony, P.S., Carr, S.D., 1997. Large lateral ramps in the Eocene Valkyr shear zone: extensional ductile faulting controlled by plutonism in southern British Columbia. Journal of Structural Geology 19, 769–784.

Spark, R.N., 1999. Crustal thickening and tectonic denudation within the Thor–Odin culmination, Monashee complex, southern Canadian Cordillera. Ph.D. thesis, University of New Brunswick.

Spear, F.S., Parrish, R.R., 1996. Petrology and cooling rates of the Valhalla complex, British Columbia, Canada. Journal of Petrology 37, 733–765.

Steiger, R.H., Jäger, E., 1977. Subcommision on geochronology: Conventions on the use of decay constants in geo- and cosmochronology. Earth and Planetary Science Letters 36, 359–362.

Tempelman-Kluit, D., Parkinson, D., 1986. Extension across the

Eocene Okanagan crustal shear in southern British Columbia. Geology 14, 318–321.

Vanderhaeghe, O., Teyssier, C., 1997. Formation of the Shuswap metamorphic complex during late-orogenic collapse of the Canadian Cordillera: role of ductile thinning and partial melting of the mid- to lower crust. Geodinamica Acta (Paris) 10, 41–58.

Wheeler, J.O., McFeely, P., compilers, 1991. Tectonic assemblage map of the Canadian Cordillera and adjacent parts of the United States of America. Geological Survey of Canada, Map 1712A.

Wheeler, J.O., Brookfield, A.J., Gabrielse, H., Monger, J.W.H., Tipper, H.W., Woodsworth, G.J., compilers, 1991. Terrane map of the Canadian Cordillera. Geological Survey of Canada, Map 1713A.

White, S.H., Burrows, S.E., Carreras, J., Shaw, N.D., Humphreys, F.J., 1980. On mylonites and ductile shear zones. Journal of Structural Geology 2, 175–187.

Williams, P.F., 1983. Large scale transposition by folding in Northern Norway. Geologische Rundschau 72, 589–604.

Williams, P.F., Campagnoni, R., 1983. Deformation and metamorphism in the Bard area of the Sesia Lanzo Zone, Western Alps, during subduction and uplift. Journal of Metamorphic Geology 1, 117–140.

Williams, P.F., Price, G.P., 1990. Origin of kinkbands and shear-band cleavage in shear zones: an experimental study. Journal of Structural Geology 12, 145–164.

Williams, P.F., Zwart, H.J. 1977. A model for the development of the Seve-Köli Caledonian nappe complex. In: Saxena, S.K., Bhattacharji, S. (Eds.), Energetics of Geological Processes. Springer-Verlag, New York, pp. 169–187.

York, D., 1969. Least squares fitting of a straight line with correlated errors. Earth and Planetary Science Letters 5, 320–324.

Zhu, X.K., O'Nions, R.K., Belshaw, N.S., Gibb, A.J., 1997. Significance of in situ SIMS chronometry of zoned monazite from Lewisian granulites, northwest Scotland. Chemical Geology 135, 35–53.